Biogeosciences
Discussions

1   **Process studies at the air-sea interface after atmospheric deposition in the Mediterranean**

2   **Sea: objectives and strategy of the PEACETIME oceanographic campaign (May-June**

3   **2017)**

4   Cécile Guieu[1], Fabrizio D'Ortenzio[1], François Dulac[2], Vincent Taillandier[1], Andrea Doglioli[3],

5   Anne Petrenko[3], Stéphanie Barrillon[3], Marc Mallet[4], Pierre Nabat[4], Karine Desboeufs[5]

6   [1] CNRS, Sorbonne Université, Laboratoire d'Océanographie de Villefranche, UMR7093,

7   Villefranche-sur-Mer, France

8   [2] Laboratoire des Sciences du Climat et de l'Environnement (LSCE), UMR 8212, CEA-CNRS-

9   UVSQ, IPSL, Univ. Paris-Saclay, CEA Saclay, Gif-sur-Yvette

10 [3] Aix-Marseille Université, CNRS, Université de Toulon, IRD, Mediterranean Institute of

11 Oceanography, UMR 7294, Marseille, France

12 4 Centre National de Recherches Météorologiques, Météo-France/CNRM/GMGEC/MOSCA,

13 Toulouse, France

14 [5] LISA (Laboratoire Interuniversitaire des Systèmes Atmosphériques), UMR CNRS 7583,

15 Université de Paris, Université Paris Est, IPSL, Créteil, France

16 **Abstract**

17 In spring, the Mediterranean Sea, a well-stratified low nutrient low chlorophyll region, receives

18 atmospheric deposition both desert dust from the Sahara and airborne particles from

19 anthropogenic sources. Such deposition translates into a supply of new nutrients and trace

20 metals for the surface waters that likely impact biogeochemical cycles. However, the

21 quantification of the impacts and the processes involved are still far from being assessed in situ.

22 In this paper, we provide a state of the art regarding dust deposition and its impact on the

23 Mediterranean Sea biogeochemistry and we describe in this context the objectives and strategy

Biogeosciences
Discussions

Open Access

EGU

24   of the PEACETIME project and cruise, entirely dedicated to filling this knowledge gap. Our

25   strategy to go a step forward than in previous approaches in understanding these impacts by

26   catching a real deposition event at sea is detailed. The PEACETIME oceanographic campaign

27   took place in May-June 2017 and we describe how we were able to successfully adapt the

28   planned transect in order to sample a Saharan dust deposition event, thanks to a dedicated

29   strategy, so-called 'Fast Action'. That was successful, providing, for the first time in our

30   knowledge, a coupled atmospheric and oceanographic sampling before, during and after an

31   atmospheric deposition event. Atmospheric and marine in situ observations and process studies

32   have been conducted in contrasted area and we summarize the work performed at sea, the type

33   of data acquired and their valorization in the papers published in the special issue.

34   1. **Introduction**

35   Understanding the exchange of energy, gases and particles at the ocean–atmosphere interface

36   is critical for the development of robust predictions of future climate change and its

37   consequences on marine ecosystems and the services they provide to society. Our

38   understanding of such exchanges has advanced rapidly over the past decade but we remain

39   unable to adequately parameterize fundamental controlling processes as identified in the new

40   research strategies of the international Surface Ocean–Lower Atmosphere Study group (Law et

41   al., 2013 and SOLAS 2015-2025: Science Plan and Organisation). A critical bottleneck is the

42   parameterization and representation of the key processes brought into play by atmospheric

43   deposition in Low Nutrient Low Chlorophyll (LNLC) regions. A perfect example of a LNLC

44   region, and of the role of the atmospheric deposition, is the Mediterranean Sea where the

45   ecosystem functioning may be modulated by pulsed atmospheric inputs in particular the

46   deposition of Saharan dust (Guieu et al., 2014a) and nutrients of anthropogenic origin (Richon

47   et al., 2018a, 2018b).

48 Indeed, the Mediterranean quasi-enclosed basin continuously receives anthropogenic aerosols

49 originating from industrial and domestic activities from all around the basin and other parts of

50 Europe, both in the western (Bergametti et al., 1989; Desboeufs et al., 2018) and eastern

51 (Tsapakis et al., 2006; Moon et al., 2016) basin. In addition to this continuous 'background'

52 inputs, the surface of the Mediterranean Sea episodically receives biomass burning particles

53 (Guieu et al., 2005) and Saharan dust (e.g. Loÿe-Pilot et al., 1986, Vincent et al., 2016). Some

54 deposition events are qualified as 'extreme events', as dust inputs as high as 22 g m^{-2} (event in

55 Nov. 2001 recorded at Ostriconi-Corsica Island, Guieu et al., 2010; event in Feb. 2002 recorded

56 at Cap Ferrat, Bonnet and Guieu, 2006) can occur on very short time scales (hours to days)

57 representing the main annual dust flux. Associated atmospheric deposition of major macro-

58 nutrient (N, P) (Kouvarakis et al., 2001; Markaki et al., 2003, 2010; Guieu et al., 2010), of iron

59 (Bonnet and Guieu, 2006) and of trace metals (Theodesi et al., 2010; Guieu et al., 2010;

60 Desboeufs et al., 2018) represents significant inputs likely supporting the primary production

61 in surface waters especially during the stratification period (Richon et al., 2018a, 2018b).

62 Among the atmospheric deposited nutrients, anthropogenic reactive nitrogen is critical on the

63 fluxes of inorganic and organic N (Markaki et al., 2010, Violaki et al., 2010). Soil dust

64 deposition plays an important role on the fluxes of P and trace metals due to the intense but

65 sporadic inputs (Bergametti et al., 1992; Guieu et al., 2010; Morales-Baquero and Perez-

66 Martinez, 2016), even if the contribution of anthropogenic aerosol deposition is significant

67 (between less of 10 % (Fe) and 90% (Zn)) (Guieu et al., 2010, Desboeufs et al., 2018). The

68 atmospheric deposition of mineral dust is correlated with dissolved trace metals enrichment of

69 the sea-surface microlayer (Cd, Co, Cu, Fe) (Tovar Sanchez et al., 2014). However, it has been

70 shown that dust deposition can result either in a net release or in scavenging of dissolved

71 inorganic phosphorus and nitrate (Louis et al., 2015) and trace elements in seawater (Wagener

72   et al., 2010; Wuttig et al., 2013; Bressac & Guieu 2013), depending on the quantity and quality

73   of in situ dissolved organic matter at the time of the deposition.

74   Recent studies in pelagic large mesocosms also allowing quantifying the export below, have

75   shown that wet Saharan dust analog deposition, by providing P and N for marine biosphere,

76   strongly stimulates primary production and phytoplanktonic biomass during several days

77   (Ridame et al., 2014; Guieu et al., 2014b; Tsagaraki et al., 2017). In addition to being strongly

78   stimulated by atmospheric P (Ridame et al., 2013), the trace metals in dust deposition have been

79   also suspected to stimulate N_2 fixation in the Mediterranean Sea (Ridame et al., 2011). The

80   extension of this fertilizing effect of dust events over the Mediterranean has been pointed out

81   from statistically positive correlations between dust deposition and surface chlorophyll

82   concentrations from remote sensing and modelling approaches (Gallisai et al., 2014). A

83   negative effect of atmospheric deposition on chlorophyll is, however, observed in the regions

84   under a large influence of aerosols from European origin (Gallisai et al., 2014). Indeed, the

85   input of anthropogenic aerosols, as Cu-rich aerosol, has been suspected to inhibit phytoplankton

86   growth (Jordi et al., 2012). Besides phytoplankton, dust deposition modifies also the bacterial

87   community structure by selectively stimulating and inhibiting certain members of the bacterial

88   community (Pulido-Villena et al., 2014; Tsagarakis et al., 2017). The budgets established from

89   4 artificial seeding experiments during project DUNE (Guieu et al., 2014b) all showed that

90   stimulating predominantly heterotrophic bacteria, atmospheric dust deposition can enhance the

91   remineralization of dissolved organic carbon (DOC), thereby reducing net atmospheric CO_2

92   drawdown. This also reduces the fraction of DOC that can be mixed and exported to deep waters

93   during the winter mixing (Pulido-Villena et al., 2008). Similarly, dust addition using on-land

94   mesocosms in the eastern Mediterranean Sea suggested that the auto- and hetero-trophic

95   components of the food web were enhanced by the dust addition thanks to the nitrogen and

96   phosphorus added through dust (Pitta et al., 2017 and companion papers) and that the response

97   was independent of the way the dust was added to the surface waters (single strong pulse or

98   three repetitive smaller pulses). One of the most intriguing results is the role of Saharan dust

99   deposition in the export of particulate organic carbon (POC) to the deep Mediterranean Sea by

100   both fertilizing and acting as ballast and facilitating aggregation processes (i.e. Ternon et al.

101   2010, Bressac et al., 2014; Desboeufs et al., 2014; Louis et al., 2017; Guieu et al., in prep.).

102   Experimental approaches have shown that wet dust deposition events, by supplying

103   bioavailable new nutrients, presents a higher positive impact compared to dry deposition, on

104   both marine primary production, nitrogen fixation and chlorophyll concentrations (Ridame et

105   al., 2014; Guieu et al., 2014b).

106   Over the past decade, most of these valuable findings have been made thanks to experimental

107   approaches based on dust and aerosols addition into bottles and up to large in-situ mesocosms

108   or using remote sensing approaches. In this paper, we provide a state of the art regarding dust

109   deposition and its impact in the Mediterranean Sea and we describe our strategy to go a step

110   forward by catching a real wet deposition event at sea in order to study in situ the effects of the

111   rapid introduction of chemical elements and particles from the atmosphere onto the marine

112   element cycles, the biology and the export of material to the deep waters.

113   **2. PEACETIME objectives**

114   In this context, the PEACETIME project (ProcEss studies at the Air-sEa Interface after dust

115   deposition in the MEditerranean sea) (http://peacetime-project.org/; last access 9 Feb. 2020)

116   aimed at extensively studying and parameterizing the chain of processes occurring in the

117   Mediterranean Sea after atmospheric deposition, especially of Saharan dust, and to put them in

118   perspective of on-going environmental changes. The ultimate goal was to assess how these

119   mechanisms impact, and will impact in the future, the functioning of the marine biogeochemical

120   cycles, the pelagic ecosystem and the feedback to the atmosphere.

121   The PEACETIME project was centered on a one-month oceanographic cruise in the central and

122   western Mediterranean Sea in May-June 2017. The strategy during the cruise was designed to

123   tackle the following questions:

124   1. How does atmospheric deposition impact trace element distribution in the column

125   water including the sea surface microlayer?

126   2. What is the role of dissolved organic matter/particulate dynamics on the fate of

127   deposited atmospheric trace elements?

128   3. How does atmospheric deposition impact biogeochemical processes and fluxes? Do in

129   situ biogeochemical /physical conditions matter?

130   4. What is the impact of atmospheric deposition on biological activity and on the

131   structure and composition of the planktonic communities?

132   5. How does atmospheric deposition impact the downward POC export and the

133   subsequent carbon sequestration?

134   6. What is the impact of biogeochemical conditions on gases and aerosol emissions from

135   the surface water?

136   7. How are optical properties above and below the air-sea interface impacted by aerosols

137   emission and dust deposition?

138   During the 33 day cruise, 40 scientists from the atmosphere and ocean communities travelled

139   2750 nautical miles (4300 km) performing simultaneously in situ sampling in the lower

140   atmosphere and the water column, and conducting on board experiments in climate reactors

141   simulating present and future marine physical conditions. The impacts on the cycles of chemical

142   elements, on marine biogeochemical processes and fluxes, on marine aerosols emission were

143   investigated in a variety of oligotrophic regimes. Characterizations of the chemical, biological,

144   physical and optical properties of both the atmosphere and the sea-surface microlayer, mixed

145   layer and deeper waters were performed.

146   The time of the campaign and the adaptive strategy for the cruise track, based on the daily

147   analysis of a number of operational forecast and near real-time observational products were

148   designed to maximize the probability to catch a Saharan dust deposition event in a stratified

149   water column in order to follow in-situ the associated processes. In this paper, we describe how

150   our strategy was designed before the campaign and how we were able to adapt it during the

151   cruise in order to sample a Saharan dust deposition event at sea, thanks to a dedicated and so-

152   called Fast Action prompted during the cruise.

153   **3.   Best time to schedule PEACETIME cruise**

154   In order to fulfil the objectives of the PEACETIME cruise, the occurrence probability of a

155   significant atmospheric deposition event was maximized by choosing to do the cruise during a

156   period of surface water stratification. This criterium matters because atmospheric inputs can be

157   the main external nutrient supply to offshore surface waters during the stratification period

158   (Guerzoni et al., 1999; The Mermex Group, 2011; Richon et al., 2018a). The Mediterranean

159   surface mixed layer depth monthly climatology (figure 1) shows a basin scale deepening from

160   November to February–March and an abrupt re-stratification in April, which is maintained

161   throughout summer and early autumn (D'Ortenzio et al., 2005). With mixed layer depths below

162   30 m in the whole Mediterranean basin, the May-September period looks particularly favorable

163   to sample highly stratified waters, with possible consideration of April and October months

164   (<40 m).

165 Because African dust transport associated to rain period generally leads to the highest

166 atmospheric deposition fluxes in the Mediterranean region (e.g., Loÿe-Pilot et al., 1986;

167 Kubilay et al., 2000; Fu et al., 2017), we checked the probability that a Saharan dust event may

168 occur during the cruise. The satellite-derived monthly climatologies of dust in the atmospheric

169 column over the Mediterranean show a maximum in summer in the western basin and in spring

170 and summer in the central basin (e.g., Moulin et al., 1998; Varga et al., 2014). Consistently,

171 model results in Figure 2 shows the highest values of dust aerosol optical depth (>0.10 and up

172 to 0.30 at 550 nm) over the whole western and central basins from May to August, an

173 intermediate situation in April and September, and the lowest values (generally <0.10) from

174 October to February. In addition to this seasonality of the dust columnar load, the climatology

175 of PM_{10} and associated African dust concentration at the surface in the Mediterranean indicates

176 that the occurrence of dust plumes close to the surface, i.e. prone to dry deposition, is maximum

177 in April-May in Greece, April-June in Sicily, May-June in continental Italy, May in SE France,

178 June-July in NE Spain and July-August in SE Spain (Pey et al., 2013). From weekly insoluble

179 deposition monitoring at 4 sites of western Mediterranean islands (Frioul, Corsica, Mallorca

180 and Lampedusa) in the period 2011-2013, Vincent et al. (2016) report that most of the most

181 intense African dust deposition events occurred between March and June.

182 Literature from deposition measurements at various sites in the western Mediterranean

183 highlights a spring maxima for dust deposition (Bergametti et al., 1989; Loÿe-Pilot and Martin,

184 1986; Avila et al., 1997; Ternon et al., 2010; Desboeufs et al., 2018). Moreover, observations

185 indicate that the highest deposition fluxes of dust are most often associated with wet deposition

186 episodes (e.g. Loÿe-Pilot et al., 1986; Bergametti et al., 1989; Guerzoni et al., 1995; Loÿe-Pilot

187 and Martin, 1996; Avila et al., 1997; Kubilay et al., 2000, Dulac et al., 2004; Guieu et al., 2009;

188 Ternon et al., 2010; Vincent et al., 2016). A survey of dust wet deposition events at Montseny

189   stations in NE Spain over 1996-2002 concluded that the maximum frequency was in May (about

190   3 events per month) and June and November (about 1 event per month). Data from Vincent et

191   al. (2016) also show that most of the two-three highest dust deposition events recorded at each

192   of the 4 island stations cited above occurred between March and May, and are most often

193   associated with rainfall.

194   It was also important that the cruise crossed different trophic regimes to get likely contrasted

195   responses to atmospheric deposition. Although the Mediterranean is classified as an

196   oligotrophic basin characterized by low-nutrient concentrations, there is a general west-to-east

197   gradient of increasing oligotrophy (The Mermex Group (2011) and references within). Figure

198   3 shows monthly averaged satellite-derived Chl-a concentrations in the Mediterranean basin :

199   from April to June, various trophic conditions can be found in the basin, with still relatively

200   "high" Chl-a concentrations (0.3 mg m^{-3}) in the Ligurian and Alboran Sea and ultra-oligotrophic

201   conditions in the central and eastern basin (< 0.03 mg m^{-3}) (Bosc et al., 2004).

202   From all the preceding considerations, we finally concluded that mid-April to mid-June was the

203   target period for the cruise.

204   **4. Spatial consideration: transect of principle of the PEACETIME cruise.**

205   The central Mediterranean Sea (MS) was our main targeted area since all the marine ecoregions

206   of the MS can be found in a relatively small zone (figure 4). Each ecoregion detected on that

207   figure presents a characteristic species association from primary producers to top predators of

208   the epipelagic domain, forced by similar environmental conditions (Reygondeau et al., 2014).

209   As seen in figure 4, the initial transect designed for PEACETIME aimed at visiting most of the

210   identified ecoregions within the 4 weeks of cruise, allowing us to test the impact of atmospheric

211   deposition on a large range of natural assemblages. The planned long stations of the transect of

212   principal were located within or at the center of 3 main ecoregions. Short stations (occupation

213   time was less than 6 hours) were positioned in order that cruising between two stations was

214   long enough (~8 hours) to allow the continuous measurement of both lower atmosphere and

215   surface seawater while cruising. Depending on atmospheric conditions during the cruise, it was

216   anticipated that one of the long station (named FAST) would be dedicated to documenting a

217   strong deposition event at sea, and that the forecasted occurrence of such an event would prompt

218   a fast action plan that might lead to change the planned transect and ship route.

219   It has to be noted that the coastal climate observatory of the Italian National Agency for New

220   Technology, Energy and Environment (ENEA) on Lampedusa Island (35°31'06"N,

221   12°37'48"E; figure 5) could provide an excellent support for atmospheric conditions in the

222   central basin before and during the cruise. Indeed, continuous measurements of aerosols

223   concentrations (Marconi et al., 2014) and composition (Becagli et al., 2012 and 2013), nutrients

224   deposition (Galletti et al., this issue), dust deposition (Vincent et al., 2016), optical

225   measurements (Meloni et al., 2007) and the vertical distribution of aerosols in the atmospheric

226   column by lidar (e.g. Di Iorio et al., 2009) are conducted at this site. During the cruise, 15

227   AERONET stations (Holben et al., 1998) plotted in figure 5 also provided continuous daytime

228   measurements of the spectral aerosol optical depth (AOD).

229   **5. Implementation of the PEACETIME cruise**

230   Based on the scientific arguments detailed above and on the availability of the ship, the

231   PEACETIME cruise was conducted during late spring conditions from May 10 to June 11, 2017

232   on board the R/V *Pourquoi Pas ?* Along the 4300 km transect, 10 short stations (with an average

233   duration of 8 hours) and 3 long stations (respectively 4 days, 4 days and 5 days duration) were

234   occupied (figure 5 and table 1).

235 Everyday, thanks to the PEACETIME Operation Center (POC; see next section) based on land,

236 the relevance to follow the initial track was discussed in the view of several types of available

237 or derived products from various operational centers producing model forecasts and near-real

238 time remote sensing products). Figure 5 represents both the planned and realized transect

239 following the day-to-day adaptive strategy.

240 5.1 **Tools for decision: the PEACETIME Operation Center**

241 Based on the experience of the ChArMEx airborne campaigns (Mallet et al., 20016) and of

242 previous oceanographic cruises needing an adaptive planning strategy based on observations

243 and short-term forecasts (see section "Satellite monitoring of the ocean"), an operational server

244 named the PEACETIME Operation Center (POC; http://poc.sedoo.fr/; last access 9 Feb. 2020)

245 was set-up by the Service de Données de l'Observatoire Midi-Pyrénées (OMP/SEDOO,

246 Toulouse, France) for the cruise. It operated from early May to mid-June 2017, gathering a set

247 of quick-looks of (i) near-real time selected remote sensing or other observational products and

248 (ii) meteorological and chemistry-transport model forecasts, considered useful for the campaign

249 planning decisions. The quick-looks were either directly transferred to the POC following their

250 production by respective operational centers, or linked from their original browser. Various

251 reports were also produced and made available on a quasi-daily basis (meteorology and dust

252 over the basin, regional and local oceanographic conditions (SPASSO; see hereafter), ship

253 trajectory...   The   complete   series   of   reports   is   available   at

254 http://poc.sedoo.fr/source/indexGarde.php?current=20170602&nav=Reports (last access 9

255 Feb. 2020). In the following, more details will be given on products that were found the most

256 useful for daily decisions during the cruise.

257 The actual positions of stations were discussed and determined on the basis of near-real time

258 satellite data analysis (SPASSO, see later) in order to account for local oceanic conditions (i.e.

259   presence or not of mesoscale structures). In parallel, short- and middle-term forecast models of

260   weather conditions and of dust transport and deposition were systematically analyzed to verify

261   the conditions, and eventually start the Fast Action. The Fast Action strategy consisted in

262   routing the ship towards an area of forecasted dust deposition event in order to tentatively

263   document the respective roles of dynamics and deposition on marine biogeochemical

264   conditions. The goal was to position the ship in the center of the area of dust deposition, at least

265   one day (24 hours) before the event in order to sample the water column before, during and

266   after the deposition, and collect and characterize the rain event. Several constraints had to be

267   considered for the Fast Action decision:

268   1. the uncertainties of the operational forecast models, which increased proportionally to

269   the length of the forecasted period;

270   2. the relative position of the ship (which was following the initial plan) and the forecasted

271   area of deposition, accounting for the maximum cruise speed of the ship (i.e. 15 knots)

272   and the need to be positioned at the station 24 h before the deposition event;

273   3. national and international authorisations related to the EEZ (Exclusive Economic

274   Zones); the Mediterranean area is almost completely submitted to national EEZ of

275   surrounding countries and, consequently, international oceanic areas are very scarce;

276   authorisation to sample an EEZ should be demanded in advance to the corresponding

277   country (generally 24 h or 48 h before, depending on the country).

278   All these elements were simultaneously analysed during a daily meeting between scientists

279   involved on land and on ship, as well as with the crew. Each day, the initial plan was confirmed

280   for the next 48 h or, eventually, modified. For most of the cruise (see figure 5), only slight

281   modifications of the initial plan were decided, as atmospheric conditions were not considered

282   favorable for the Fast Action. They dramatically changed on the 28th of May, during the

283   sampling of the ION station, conducting to the decision to start the Fast Action. The sequence

284   of events leading to the Fast Action are described later.

Atmospheric conditions

286   Several near-real time remote sensing products and model forecasts were used. In terms of

287   aerosol remote sensing, we mainly relied on two products. The first one was the aerosol optical

288   depth at 550 nm (AOD_{550}) distribution over the sea, as produced in near-real time by the ICARE

289   data and service centre, Lille, France (product SEV_AER-OC-L2; http://www.icare.univ-

290   lille1.fr/projects/seviri-aerosols; last access 9 Feb., 2020). Data from the Spinning Enhanced

291   Visible and Infra-red Imager (SEVIRI) on-board the geostationary satellite Meteosat Second

292   Generation (MSG) are directly acquired every 15 min by the Service d'Archivage et de

293   Traitement Météorologique des Observations Satellitaires of the Centre de Météorologie

294   Spatiale (CMS/SATMOS), Lannion, France, and processed within hours by ICARE based on

295   the algorithm of Thieuleux et al. (2005). The MSG satellite position at 0° longitude allows a

296   good coverage for aerosol climatologies and case studies of aerosol transport over the

297   Mediterranean basin (e.g. figure I.19 in Lionello et al., 2012; Chazette et al., 2016 and 2019)

298   and surrounding continental regions (Carrer et al., 2014) as well as of desert dust source regions

299   in Africa (e.g. Gonzales and Briottet, 2017). In addition to the quick-look from the level-2

300   product (SEV_AER-OC-L2) available between 4:30 and 18:00 UT at the maximum in mid-

301   June in our area of interest, a daily mean level-3 (SEV_AER-OC-D3) is produced every night

302   by averaging all available time slots during the previous day between 4:00 and 19:45 UT. Figure

303   6 illustrates this product for the 3rd of June when an African dust plume from North Africa

304   associated to a cloudy air mass invaded the westernmost Mediterranean basin atmosphere. The

305   horizontal resolution of the product is of 3 x 3 km^2 at nadir, of the order of 12.5 km^2 in the

306   Alboran Sea, 15 km^2 in the North of the Gulf of Genova, and 18 km^2 in the northeasternmost

307   basin (about 13.07, 13.64, and 13.96 at the FAST, ION, and TYR station, respectively).

308   Although less accurate than AOD from MODIS when compared to AERONET data, the high

309   temporal resolution of MSG/SEVIRI-derived AOD offers a much better daily coverage of the

310   area than any orbiting satellite (Bréon et al., 2011), especially when partial cloud coverage can

311   be compensated thanks to successive images, as illustrated in figure 6.

312   The second useful remote sensing product was the North African Sand Storm Survey

313   (NASCube) also produced from MSG/SEVIRI, at the Laboratoire d'Optique Atmosphérique,

314   Lille, France (http://nascube.univ-lille1.fr; last access, 9 Feb. 2020). It generates continuous

315   day and night images of desert dust plumes over the northern African continent and Arabian

316   Peninsula, using an artificial neural network methodology producing colour composite images

317   by processing 8 visible, near-infrared and thermal infrared bands of SEVIRI (Gonzales and

318   Briottet, 2017). Figure 7 shows a window of this product for the 1st June 2017, showing the

319   probable dust source regions (south of Morocco and western Algeria) of the plume found the

320   following days over the westernmost Mediterranean basin as seen in figure 6.

321   During the campaign, we also used on a regular basis air mass trajectories computed with the

322   Hysplit tool of the Air Resources Laboratory of the National Ocean and Atmosphere

323   Administration (NOAA/ARL; https://ready.arl.noaa.gov/HYSPLIT_traj.php; last access 9 Feb.

324   2020; Stein et al., 2015; Rolph et al., 2017) based on global meteorological 192-h forecasts

325   from the Global Forecasting System (GFS) model (1-deg, 3-h resolution) operated by the

326   National Centers for Environmental Prediction (NCEP; Yang et al., 2006). It could be used both

327   in forward mode to forecast the transport over the western Mediterranean of dust plumes

328   detected over Africa by NASCube, and in backward mode to identify the origin of air masses

329   over the ship position.

330   In addition to aerosol remote sensing observations we also used near real time rainfall remote

331   sensing produced by the Meteo Company, an international weather network

332   (https://meteoradar.co.uk; last access 9 Feb. 2020) providing every 15 mn real time weather

333   radar- and satellite-derived maps of precipitation, clouds, and lightning on a European window

334   covering most of the Mediterranean basin (north of 32°N or 35.5°N, depending on products).

335   The satellite infrared images from SEVIRI are filtered to show the thicker clouds, and

336   observations from 45 European rain radar are integrated. Figure 8 illustrates the combined

337   SEVIRI satellite and radar product showing both clouds, precipitation and lightning for two

338   time slots on 3 June 2017. They show the beginning and the end, respectively, of a convective

339   rainfall of low intensity (<2 mm h-1) between Algeria and Spain in the dusty and cloudy area

340   visible in Figure 6 west of the ship.

341   A number of operational forecast models were also used, both for weather forecast and aerosol

342   transport. In order to understand the synoptic circulation, we especially considered surface

343   pressure (P) and 500-hPa (about 5.5-km altitude) geopotential ($Z500$) maps over the European

344   domain covering the whole Mediterranean basin and northern Atlantic from the global

345   numerical weather prediction model ARPEGE (Courtier and Geleyn, 1988), developed and

346   maintained at Météo-France. Its horizontal resolution varies from 7.5 km in France to 37 km

347   over Southern Pacific, and four daily forecasts including data assimilation are carried out every

348   day (available by http://www.meteociel.fr, last access 9 Feb. 2020). Because we were

349   especially targeting possible aerosol deposition events, we also analysed daily a set of up to 5-

350   days, 1-, 3-, or 6-hourly depending on models, precipitation forecasts from several models

351   including those made available by meteociel.fr including global weather forecast models such

352   as ARPEGE, IFS (the model developed at ECMWF; Barros et al. 1995), the Canadian CMC-

353   MRB GEM model (Côté and Gravel, 1998), the GFS atmospheric model from NCEP

354   (Kanamitsu, 1989) and its ensemble GEFS, but also the regional non-hydrostatic model

355   AROME (Seity et al., 2011) for the NW Mediterranean only at 1.3 km resolution.

356   Three regional dust transport models have also been considered, namely SKIRON operated by

357   the Atmospheric Modeling and Weather Forecasting Group (AM&WFG) of the University of

358   Athens (Kallos et al., 2009; Spyrou et al., 2010) and the two models NMMB-BSC (Non-

359   Hydrostatic Multiscale Model; Pérez et al., 2011) and BSC-DREAM8b (Basart et et al., 2012)

360   operated by the Barcelona Supercomputing Centre (BSC). SKIRON and BSC-DREAM8b have

361   a horizontal resolution of 0.24° and 0.33°, respectively, and are both initialized and constrained

362   at their boundaries by NCEP/GFS 6-hourly data. NMMB-BSC regional model has a resolution

363   of 0.47° x 1/3° and is constrained by the NCEP global version of the model (Pérez et al., 2011).

364   In terms of dust transport modeling, we mainly relied on 6-hourly dust optical depth and dry

365   and wet dust deposition fluxes forecasted daily from 12 UTC over the next 72 h by the NMMB-

366   BSC-Dust and BSC-DREAM8b v2.0 models and over the next 180 h (5.5 d) by SKIRON.

367   Because of its longer temporal range of forecast, the wet dust deposition product by SKIRON

368   was particularly useful to issue an early pre-alert for the Fast Action during the cruise. Figure

369   9 compares the forecast maps of 6-h accumulated dust deposition flux at 4 time steps from 3rd

370   June 2017 12 UTC to 5 June 00 UTC, from the 2nd June runs of those 3 models. This period

371   corresponds to the scavenging of the dust plume shown in Figure 6 that was targeted for the

372   Fast Action (see below).

373   We also used a set of forecast of aerosol or dust optical depth from a series of models: (i) 60-h,

374   6-hourly ensemble and comparative forecasts of dust optical depth from models operated by

375   the BSC for the World Meteorological Organization (WMO) Sand and Dust Storm Warning

376   Advisory and Assessment System (SDS-WAS), and made available by the Spanish Agencia

377   Estatal de Meteorologia (AEMET; https://sds-was.aemet.es/forecast-products/dust-forecasts/;

378   last access 9 Feb. 2020; it is worth noting that Basart et al. (2016) model data comparison over

379   summer 2012 showed better average performances of the model ensemble dust forecasts

380   compared to forecasts from any individual model (ii) 5-days, 3-hourly dust and sulphate AOD

381   Copernicus/GMES products over Europe and North Africa produced by the European Center

382   for Medium-Range Forecast (ECMWF), and (iii) 114-h, 6-hourly sulfate, dust and smoke AOD

383   over Europe and the Mediterranean region north of 35°N from the Naval Research Laboratory

384   (NRL) global NRL Aerosol Analysis and Prediction System (NAAPS) model that is using an

385   AOD assimilation package (Zhang et al., 2008); further, we used the kml formatted animations

386   of the NAAPS 5-days global forecasts of AOD projected on a GoogleEarth satellite view

387   centered on the western Mediterranean, which shows areas with significant AOD (>0.1) of

388   sulfate, dust or smoke. Finally, we also considered the daily maps (at time 00 UTC) produced

389   by the Earth Wind Map community (https://earth.nullschool.net; last access 9 Feb. 2020),

390   consisting of AOD from sulfate or dust from the NASA Global Modeling and Assimilation

391   Office (GMAO) Goddard Earth Observing System version 5 (GEOS-5) model overlaid by

392   surface or 700 hPa winds from the GFS model in order to check the dominant aerosol type and

393   transport conditions at the ship position.

394   **Ocean conditions**

395   Concerning the surface ocean, several remote-sensing datasets were exploited using the

396   SPASSO (Software Package for an Adaptive Satellite-based Sampling for Ocean campaigns

397   https://spasso.mio.osupytheas.fr/; last access: 9 Feb. 2020) in order to guide the cruise through

398   a Lagrangian adaptive sampling-strategy aiming at avoiding region of complex circulation and

399   dynamics (fronts, small scale eddies). The idea behind this approach was to aim at a situation

400   where the air-sea exchanges dominate and lateral advection and diffusion can be neglected.

401   Such an approach was already successfully adopted during several previous cruises such as

402   LATEX (Nencioli et al., 2011; Doglioli et al., 2013, Petrenko et al., 2017), KEOPS2 (d'Ovidio

403   et al., 2015), OUTPACE (Moutin et al., 2017; de Verneil et al., 2018) and OSCAHR (Rousselet

404   et al., 2019). During PEACETIME, we used the following datasets: (1) altimetry data from the

405   AVISO Mediterranean regional product (https://www.aviso.altimetry.fr/data/products/sea-

406   surface-height-products/regional/mediterranean-sea-gridded-sea-level-heights-and-derived-

407   variables.html); the altimetry-derived currents were then processed by SPASSO to derive

408   Eulerian and Lagrangian diagnostics of ocean circulation: Okubo-Weiss parameter, particle

409   retention time and advection, Finite Size Lyapunov Exposant (e.g. figure 10); (2) the sea surface

410   temperature (level 3 with resolutions of 4 and 1 km) and (3) the chlorophyll concentration (level

411   3 with a resolution of 1 km, MODIS Aqua and NPPVIIRS sensors combined after May 27,

412   2017 into a unique product) provided by CMEMS - Copernicus Marine Environment

413   Monitoring Service (http://marine.copernicus.eu/).

414   **5.2 The Fast Action**

415   **The decision process and atmospheric conditions**

416   On the 28th of May, the ship was ending the long station ION in the Ionian Sea under a

417   continuing northern atmospheric flux. A low pressure system reaching Spain from the Atlantic,

418   a typical situation for African dust transport in summer in this area (Moulin et al., 1998) caused

419   a southern flux over the western basin. But no significant emission of dust was yet detected in

420   Africa with NASCube. Aerosol transport models forecasted, however, the presence of dust

421   plume of moderate intensity for the following days, mainly confined to the southern part of the

422   western Mediterranean basin following a persistent western flux for several days limiting the

423   extension of dust transport towards the north of the basin. Some dust was predicted by NMMB-

424   BSC and SKIRON model runs of 27 June to be deposited by rain south of the Balearic islands

425   on 30 and 31 May, but meteorological forecasts did not converge on the time and location of

426   precipitation. In addition, the possible area of dust deposition was far from the ship, 16° in

427   longitude west from the ION station. Consequently, no modification of the initial plan was

428   decided and the station 8 was carried out southwest of Sicily on 30 May.

429   At the end of station 8 on 30th May, satellite observations confirmed the presence of atmospheric

430   dust in a cloudy air mass over the western part of the Mediterranean and long-term predictions

431   of AOD indicated the continuing presence of dust over the Alboran Sea, with a new dust plume

432   likely extending northwest on June 2 or 3. Although models still diverged in forecasting rain

433   over this region, the southwestern part of the Mediterranean basin looked to be the most dusty

434   area for the next days and it was decided to modify the initial plan and to move towards the

435   west for the last part of the cruise (see figure 5, the long transect south of Sicily).

436   The 31th of May the ship reached a position approximately located between Sicily and Sardinia

437   islands. Significant dust emissions were again observed over North Africa from the night of 30-

438   31 May on, and the predictions for a new significant dust event over the southwestern

439   Mediterranean on June 3-5 were confirmed. Although the differences between the models were

440   still important (only SKIRON forecasted a wet deposition event south of Spain for the 3-4th of

441   June), it was decided to continuously move the ship westward, and to shift station 9 from its

442   initial position in the Tyrrhenian Sea to a new position in the Alboran Sea. We considered that

443   another station in the Tyrrhenian area was not critical for the cruise objectives and that

444   establishing the area of next operations in the Alboran Sea could facilitate the re-positioning of

445   the ship in the case of a confirmed prediction of a wet deposition event.

446   The 1st of June, during the sampling at station 9 midway between Sicily and Spain, it was

447   decided to start the Fast Action. Indeed, dust emissions continued in Algeria and southern

448   Morocco associated to a southern flux, aerosol transport models confirmed a new significant

449   dust episode with AOD >0.8 (i.e. roughly 1 g m^{-2} of dust in the atmospheric column) for June

19

450   3-5, and the occurrence of associated rains appeared most likely from most meteorological

451   forecasts. SKIRON and NMMB-BSC predicted the dust wet deposition flux to be more

452   important on 3rd June in the Alboran Sea west of 0° longitude, of the order of 1.5 and 0.5 g m$^-$

453   ^{2}, respectively), but longer-term forecasts by SKIRON predicted wet dust deposition more east

454   south of the Balearic Islands on June 4 (~0.5 g m^{-2}) and especially on first half of June 5

455   (possibly >1.5 g m^{-2}), a possibility confirmed by other rain forecasts. The Fast Action station

456   was positioned 145 km south the Balearic Island of Mallorca and 126 km north of the Algerian

457   coast (Figure 5), where a limited portion of the sea is part of international waters (i.e. not

458   included in an EEZ), and in an area where the influence of Atlantic waters reacher in nutrients

459   than Mediterranean waters should be limited compared to the more western Alboran Sea. The

460   ship reached the FAST station location on the 2nd of June at the end of the day (Table 1) and

461   the ocean and atmospheric sampling started immediately.

462   Although cloudy, only from the 3rd of June rain conditions were observed in the neighbouring

463   area (see rain radar composite images in figure 11). The SEVIRI AOD remote sensing

464   confirmed the export of a dust plume from North Africa south of the Balearic Islands with high

465   AOD (>0.8; Figure 6) and NASCube confirmed new dust emissions in the night from 3 to 4

466   June. The dust plume was transported to the NE up to Sardinia on June 4, with AOD <0.5 in all

467   the area and clear sky with low AOD was left west of 4°E on June 5 (Desboeufs et al., in

468   preparation, this issue). Wet deposition of dust for the 4th and early 5th June in the FAST station

469   area were confirmed by the deposition maps from the 3 regional dust transport model forecast

470   runs of June 2, although with decreasing intensity compared to the previous runs (except for

471   BSC-DREAM8b that did not forecast dust wet deposition in earlier run), from a very small flux

472   of a few mg m^{-2} (BSC-DREAM8b) to about 100 mg m^{-2} (NMMB-BSC) and up to more than 1

473   g m^{-2} (SKIRON) (Figure 9). A rain front, moving eastward from Spain and North Africa

474   regions, reached the Fast Action position the night between the 4th and the 5th of June (Figure

475   11). A single event of rain was observed and sampled on the ship at the station FAST on 5th

476   June from 2:36 am to 3:04 am. Continuous lidar measurements on board the ship confirmed the

477   presence of a dust layer mainly over the atmospheric boundary layer over the FAST station and

478   its below-cloud deposition during the rain event of early 5th June (Desboeufs et al., in

479   preparation, this issue). The chemical composition of this rain sample confirmed wet deposition

480   of dust reaching a total particulate flux of 12 mg.m^{-2} (Fu et al., in preparation, this issue), which

481   is among the lowest most intense dust deposition fluxes recorded in this area from long time-

482   series of deposition network (Vincent et al., 2016).

483   **Sea Surface dynamic context at FAST**

484   Several approaches have been implemented to highlight the dynamical context around the

485   FAST station in the waters above 200m, the physical structures and the possible influences of

486   the dynamics on the stability of the water masses at the station. These approaches are based on

487   in situ observations (Moving Vessel Profiler (VMP) transect and drifters trajectories) and

488   diagnostic tools.

489   On board, a MVP collected high frequency Conductivity- Temperature- Depth (CTD) data

490   along two transects: the first one when the vessel approached the FAST station from the east,

491   before the station took place, and the second one west of the FAST station, on the transect back

492   from station 10. Figure 12 shows these data in a longitude-depth section. To the east of the

493   FAST station the surface water was colder and saltier than to the west, where a strong

494   deformation of the isopycnals suggests the presence of an Algerian anticyclonic eddy. Such

495   eddy carries recent Atlantic water and generates a southward current that only partially impacts

496   the FAST station area.

497   The post-cruise comparison of the hull-mounted ADCP data combined with the SVP drifters

498   trajectories and the altimery-derived currents shows a good agreement all along the cruise and

499   in particular at the FAST station (Figure 12). Moreover, the agreement between SVP and

500   numerical particle trajectories has been slightly improved when we also took into account the

501   Ekman drift calculated with wind data from the high resolution regional model WRF 3.7.

502   This allowed us to calculate backward trajectories of the surface water masses using the

503   ARIANE Lagrangian tool (Blanke and Raynaud, 1997; Blanke et al., 1999) in order to estimate

504   the origins of the sampled surface water at the LD stations. As seen from the repeated CTDs

505   (see previous section), at the FAST station a southward current associated to the large Algerian

506   eddy was present. We estimated that over the whole station duration, a mean value of 57(26)%

507   of water remained in the station zone after 1(2) day(s). Moreover, combining the particle

508   trajectories and the precipitation data from the WRF 3.7 model we concluded that the rain,

509   which fell slightly upstream the LD-FAST station in the previous days, likely impacted the

510   sampled water mass (figure 14).

511   **Temporal evolution of surface seawater properties during FAST**

512   Station FAST has been documented at its fixed point during seven days by 43 repeated CTD

513   casts in the depth range 0-200 m.

514   The hydrological situation was characterized by a very shallow surface mixed layer and a sharp

515   seasonal thermocline that extended underneath down to 75 m depth (Figure 15, upper right and

516   middle right panels). In this upper layer, salinity values were lower than 37.5, which is

517   characteristic of modified Atlantic waters flowing eastward inside the Mediterranean Sea. In

518   the deeper layers, salinity increased sharply with depth until 350 m where it reached its

519   maximum value (38.59), which is characteristic of Levantine intermediate waters flowing

22

520   westward into the Mediterranean outflow. Deep waters, formed at winter convection zones of

521   the northwestern Mediterranean, had lower salinity values (38.48); they extended from 1400 m

522   down to the sea bottom.

523   The hydrological conditions at this site between June 2 and 8 during the Fast Action mainly

524   evolved in the upper layer (Figure 15, upper left and middle left panels). The surface mixed

525   layer was shallow with variations from 9-m to 19-m depth following the diurnal cycle. Mixed

526   layer salinity remained equal until the 7th of June; in particular no dilution effect due the rainfall

527   on 3rd June has been recorded. The stratification of the whole water column remained steady

528   during the long station. Density horizons kept lain along isobars in the upper layer, which signs

529   the absence of geostrophic perturbations during the long station. However, the current profilers

530   indicated a depth-independent (barotropic) motion of amplitude 3 cm s^{-1} heading 220°, which

531   is in agreement with the position of the station within the large eastern Algerian Gyre, a

532   component of the basin scale cyclonic circulation described by Testor et al. (2005). This

533   southwestward flow transported superficial water masses of distinct properties as clearly

534   marked below the mixed layer by salinity anomalies (referenced to the initial profile of 2nd June

535   16:30). These water masses crossed the observation site, disrupting the water column in the

536   depth range of 25-100 m, lowering salinity values by 0.1 in the extension of the thermocline

537   and increasing salinity values by 0.05 underneath. Although clearly present, this hydrological

538   anomaly did not affect the surface waters and the MLD was stable during the Fast Action

539   precluding any input from below that could have been linked to destratification induced by

540   strong wind associated to the dust event as hypothesized in Guieu et al. (2010) from time-series

541   observations in the northwestern Mediterranean Sea. Such conditions are favorable to observe

542   any change strictly attributed to external inputs from above (i.e. atmospheric deposition).

543   The distribution of phytoplanktonic biomass has been detected by optical sensors mounted in

544   the CTD package (Figure 15 lower panels): measurements of fluorescence and of beam

545   transmission provided similar patterns, stressing the biogenic character of particles present in

546   the water column. Intermittent signal at the sea surface has been detected only by

547   transmissometry, however no clear relationship with the rainfall event can be stated (see the

548   first profile after event in red). The vertical distribution was displayed as a deep chlorophyll

549   maximum of about 20-m thickness, located at the base of the thermocline (about 75 m). Short-

550   term evolution during the seven days of observation displayed variations in intensity and depth

551   of the deep chlorophyll maximum, as well as splitting and merging sequences of the peak. Such

552   perturbations appeared after the rainfall event of the 3rd June, however they more likely result

553   from the intrusion of water masses from north at this depth range. This hypothesis is reinforced

554   by the absence of any geostrophic perturbation in the density time series that could have injected

555   biomass or nutrients via diapycnal processes. Another candidate could be the mixing effect

556   associated to the breaking of internal gravity waves that propagated along the thermocline.

557   5.3 Work at stations and work underway

558   In the figure 16 we show the satellite-derived SST data averaged taking into account the ship

559   position. During the cruise a general warming of the sea surface is observed and the FAST

560   station has been performed in waters warmer than the two others LD stations.

561   Chlorophyll concentrations as seen by satellite over the western and central Mediterranean Sea

562   were typical of the oligotrophic conditions encountered during the season characterized by a

563   strong stratification (Figure 17). The west-east gradient between oligotrophic to very

564   oligotrophic was clearly established and minimal concentrations (about 0.05 mg m^{-3}) were

565   observed in the Ionian Sea.

566   Surface inorganic nutrients measured at nanomolar concentrations were very low for both

567   dissolved inorganic nitrogen (DIN) and phosphorus (DIP). Indeed, average concentration in 0-

568   20 m layer was 90 nM DIN and 15 nM DIP at the westernmost station (station 10) and 14 nM

569   DIN and 10 nM DIP at the easternmost station (ION). Along the longitudinal transect, a

570   deepening of the nutrient depleted layer toward the east was observed (figure 18) consistent

571   with the general trend of those nutrients in the Mediterranean basin as described in Mermex

572   Group (2011) and references inside.

573   All along the cruise, the work at sea was divided between short (~8 hours) and long (up to five

574   days) stations to allow both a good description of the different ecoregions crossed and to

575   perform process studies. The number of short stations was the best compromise in order to (1)

576   allow at least 8 hours of transect at 9 knots in between 2 short stations, necessary for a good

577   continuous monitoring of both low atmosphere and surface waters while cruising and (2) to

578   have enough short stations to describe well enough stocks and fluxes along the whole column

579   water and microstructure of the mixed layer in the contrasted biogeochemical regions crossed.

580   Long stations were located in 3 different ecoregions (see Figure 3) characterized by different *in*

581   *situ* conditions (see figures 16 & 17) all characterized by oligotrophic conditions. The duration

582   of the long stations (4 days at TYR and ION and 5 days at FAST; table 1) allowed process

583   studies both in situ (drifting mooring supporting different types of traps and instruments) and

584   on board (artificial dust seeding experiment in 300 L climate reactors; see below). Table 2

585   summarizes the operations conducted during the cruise and the parameters obtained, (1) on a

586   continuous basis, (2) at short stations, and (3) at long stations . A summary of the use of those

587   parameters in the different papers presented in this Special Issue and in other papers is also

588   given in that table.

589 **6. Conclusion**

590   The PEACETIME oceanographic expedition conducted in spring 2017 cruised over a 20°

591   longitudinal gradient across the western and central Mediterranean Sea during the season

592   characterized by strong stratification, low productivity and high chance to be submitted to dust

593   wet deposition. Those conditions were required in order to fulfil the objectives of the project

594   aiming at quantifying the biogeochemical processes at play after atmospheric deposition and its

595   impact on ecosystem functioning. Thanks to an adaptive strategy based on a large panel of

596   atmosphere and ocean real time observations and forecast models, the track of the cruise was

597   optimized from day to day. In particular, we were successful to timely reroute the R/V toward

598   an area where dust deposition was expected and actually observed and sampled. Different

599   atmospheric situations were encountered during the cruise, allowing the acquisition of a large

600   dataset under different dynamical and biogeochemical in situ conditions to explore the chemical

601   and ecosystem in situ response to deposition.

602   **Acknowledgments**

612   the station FAST. We finally acknowledge the technical help of the many teams supporting

613   operational production of model forecasts and remote sensing products that contributed to the

614   POC and were the basis of our daily briefings and decision for the Fast Action, especially

615   Jacques Descloitres for MSG-derived AOD, Louis Gonzalez for NASCube products, and

616   Christos Spyrou for SKIRON forecasts.

617   **Author contribution:** CG and KD designed the PEACETIME project. FD and FDO analyzed

618   the FAST Action. FD, MM and PN analysed the atmospheric components and VT, AD, AP and

619   SB analysed the marine components. CG prepared the manuscript with contributions from all

620   co-authors.

621   **References**

622   1.   Avila, A., Queralt-Mitjans, I., & Alarcón, M. (1997) Mineralogical composition of
623   African dust delivered by red rains over northeastern Spain, J. Geophys. Res., 102,
624   21977-21996, doi:10.1029/97JD00485.

625   2.   Barbieux M., Uitz J., Mignot A., Gentili B., Roesler C., Loisel H., Poteau A.,
626   Schmechtig C., Taillandier V., Leymarie E., Penkerc'h C., Claustre H., D'Ortenzio F.
627   & Bricaud A., Subsurface biological production in the Mediterranean Sea: Estimates
628   based on the diel cycle of optical properties measured by BGC-Argo floats, in
629   preparation (this special issue)

630   3.   Barros, S.R.M., Dent, D., Isaksen, L., Robinson, G., Mozdzynski, G., & Wollenweber,
631   F. (1995) The IFS model: A parallel production weather code, Parallel Computing, 21,
632   1621-1638, doi:10.1016/0167-8191(96)80002-0.

633   4.   Basart S., F. Dulac, J.M. Baldasano, P. Nabat, M. Mallet, F. Solmon, B. Laurent, J.
634   Vincent, L. Menut, L. El Amraoui, B. Sic, J.-P. Chaboureau, J.-F. Léon, K.
635   Schepanski, J.-B. Renard, F. Ravetta, J. Pelon, C. Di Biagio, P. Formenti, I. Chiapello,
636   J.-L. Roujean, X. Ceamanos, D. Carrer, M. Sicard, H. Delbarre, G. Roberts, W.
637   Junkermann, & J.-L. Attié (2016) Extensive comparison between a set of European
638   dust regional models and observations in the western Mediterranean for the summer
639   2012 pre-ChArMEx/TRAQA campaign, In Air Pollution Modeling and its Application

640   XXIV, D.G. Steyn and N. Chaumerliac Eds., Springer Series Proc. in Complexity, 79-
641   83, doi:10.1007/978-3-319-24478-5_13.
642   5.   Basart S., Pérez, C., Nickovic, S., & Baldasano, J.M. (2012) Development and
643   evaluation of the BSC-DREAM8b dust regional model over Northern Africa, the
644   Mediterranean and the Middle East, Tellus, 64, 18539,
645   doi:10.3402/tellusb.v64i0.18539.
646   6.   Becagli, S., Lazzara, L., Fani, F., Marchese, C., Traversi, R., Severi, M., di Sarra, A.,
647   Sferlazzo, D. M., Piacentino, S., 461 Bommarito, C., Dayan, U., and Udisti, R. (2013)
648   Relationship between methanesulfonate (MS−) in atmospheric 462 particulate and
649   remotely sensed phytoplankton activity in oligo-mesotrophic central Mediterranean
650   Sea, 463 Atmospheric Environment, 79, 681-688,
651   https://doi.org/10.1016/j.atmosenv.2013.07.032
652   7.   Becagli, S., Sferlazzo, D. M., Pace, G., di Sarra, A., Bommarito, C., Calzolai, G.,
653   Ghedini, C., Lucarelli, F., Meloni, D., Monteleone, F., Severi, M., Traversi, R., and
654   Udisti, R. (2012): Evidence for heavy fuel oil combustion aerosols from chemical
655   analyses at the island of Lampedusa: a possible large role of ships emissions in the
656   Mediterranean, Atmos. Chem. Phys., 12, 3479-3492, 10.5194/acp-12-3479-2012.
657   8.   Bergametti G., E. Remoudaki, R. Losno, E. Steiner, B. Chatenet, & P. Buat-Ménard
658   (1992) Source, transport and deposition of atmospheric phosphorus over the
659   northwestern Mediterranean, Journal of Atmospheric Chemistry, 14, 501-513,
660   doi:10.1007/BF00115254.
661   9.   Bergametti, G., Dutot, A. L., Buat-Ménard, P., Losno, R., & Remoudaki, E. (1989)
662   Seasonal variability of the elemental composition of atmospheric aerosol particles
663   over the Northwestern Mediterranean, Tellus, 41B, 353-361, doi:10.1111/j.1600-
664   0889.1989.tb00314.x.
665   10. Berline L, Doglioli AM, Petrenko A, Barrillon S, Simon-Bot F & Carlotti F, Sharp
666   gradient in particle load at the boundary between Modified Atlantic Water and Ionian
667   Surface Water, Central Ionian Sea, in preparation (this special issue)
668   11. Blanke, B., & Raynaud, S. (1997) Kinematics of the Pacific equatorial undercurrent:
669   An Eulerian and Lagrangian approach from GCM results, Journal of Physical
670   Oceanography, 27, 1038-1053, doi:10.1175/1520-
671   0485(1997)027<1038:KOTPEU>2.0.CO;2.

672   12.   Blanke, B., Arhan, M., Madec, G., & Roche, S. (1999) Warm water paths in the
673   equatorial Atlantic as diagnosed with a general circulation model, Journal of Physical
674   Oceanography, 29, 2753-2768, doi:10.1175/1520-
675   0485(1999)029<2753:WWPITE>2.0.CO;2.
676   13.   Bonnet, S., & Guieu, C. (2006) Atmospheric Forcing on the Annual Iron Cycle in the
677   Mediterranean Sea. A one-year Survey. Journal of Geophysical Research, 111,
678   C09010, doi:10.1029/2005JC003213.
679   14.   Bosc, E., Bricaud, A., & Antoine, D. (2004) Seasonal and interannual variability in
680   algal biomass and primary production in the Mediterranean Sea, as derived from 4
681   years of SeaWiFS observations, Global Biogeochemical Cycles, 18, GB1005,
682   doi:10.1029/2003GB002034.
683   15.   Brandt M.I, Trouche B., Quintric L., Wincker P., Poulain J., Arnaud-Haond S., A
684   flexible pipeline combining bioinformatic correction tools for prokaryotic and
685   eukaryotic metabarcoding. https://doi.org/10.1101/717355, submitted, 2019
686   16.   Brandt M.I., Zeppilli D., Simier M., Guenther B., Trouche B., Henry N., Orejas C.,
687   Pradillon F., Fabri M-C, Cambon-Bonavita A-M, Guieu C., Quintric L., Belser C.,
688   Poulain J., Wincker P., Maignien L., de Vargas C., & Arnaud-Haond S., Multi-marker
689   eDNA metabarcoding reveals large and small-scale metazoan biodiversity patterns in
690   the deep-sea Atlantic-Mediterranean transition zone, in preparation.
691   17.   Bréon, F.-M., Vermeulen, A., & Descloitres, J. (2011) An evaluation of satellite
692   aerosol products against sunphotometer measurements, Remote Sensing of
693   Environment, 115, 3102-3111, doi:10.1016/j.rse.2011.06.017.
694   18.   Bressac M, Wagener T, Tovar-Sanchez A, Ridame C, Albani S, Fu F, Desboeufs K &
695   Guieu C, Residence time of dissolved and particulate trace elements in the surface
696   Mediterranean Sea (Peacetime cruise), in preparation (this special issue)
697   19.   Bressac M., C. Guieu, D. Doxaran, F. Bourrin, N. Leblond K. Desboeufs & C. Ridame
698   (2014) Quantification of the lithogenic carbon pump following a simulated dust
699   deposition event in large mesocosm, Biogeosciences, 11, 1007-1020, doi:10.5194/bg-
700   11-1007-2014.
701   20.   Bressac M., C. Guieu, M. J. Ellwood, A. Tagliabue, T. Wagener, E. C. Laurenceau
702   Cornec, H. Whitby, G. Sarthou, & P. W. Boyd. (2019) Resupply of mesopelagic
703   dissolved iron controlled by particulate iron composition. Nature Geoscience, 12(12),
704   995:1000, doi:10.1038/s41561-019-0476-6.

705   21.   Bressac, M., & Guieu, C. (2013) Post-depositional processes: What really happens to
706   new atmospheric iron in the ocean surface? Global Biogeochemical Cycles, 27, 859-
707   870, doi:10.1002/gbc.20076.

708   22.   Carrer D., X. Ceamanos, B. Six, & J.-L. Roujean (2014) AERUS-GEO: A newly
709   available satellite-derived aerosol optical depth product over Europe and Africa,
710   Geophysical Research Letters, 41, 7731-7738, doi:10.1002/2014GL061707.

711   23.   Chazette, P., Totems, J., & Shang, X. (2019) Transport of aerosols over the French
712   Riviera – link between ground-based lidar and spaceborne observations, Atmospheric
713   Chemistry and Physics, 19, 3885–3904, doi:10.5194/acp-19-3885-2019.

714   24.   Chazette, P., Totems, J., Ancellet, G., Pelon, J., & Sicard, M. (2016) Temporal
715   consistency of lidar observations during aerosol transport events in the framework of
716   the ChArMEx/ADRIMED campaign at Minorca in June 2013, Atmospheric
717   Chemistry and Physics, 16, 2863–2875, doi:10.5194/acp-16-2863-2016.

718   25.   Côté, J., S. Gravel, A. Méthot, A. Patoine, M. Roch, & A. Staniforth, 1998: The
719   Operational CMC–MRB Global Environmental Multiscale (GEM) Model. Part I:
720   Design Considerations and Formulation. Mon. Wea. Rev., 126, 1373–1395,
721   doi:10.1175/1520-0493(1998)126<1373:TOCMGE>2.0.CO;2.

722   26.   Courtier, P. & Geleyn, J.-F. (1988) A global numerical weather predic-tion model with
723   variable resolution: Application to the shallowmodel equations, Q. J. Roy. Meteor.
724   Soc., 114, 1321–1346, doi:10.1002/qj.49711448309.

725   27.   de Verneil, A., Rousselet, L., Doglioli, A. M., Petrenko, A. A., Maes, C., Bouruet-
726   Aubertot, P., & Moutin, T. (2018) OUTPACE long duration stations: physical
727   variability, context of biogeochemical sampling, and evaluation of sampling strategy,
728   Biogeosciences, 15, 2125–2147, doi:10.5194/bg-15-2125-2018.

729   28.   Desboeufs K, J.-F. Doussin, C. Giorio, S. Triquet, F. Fu, D. Garcia-Nieto, F. Dulac, A.
730   Féron, P. Formenti, F. Maisonneuve, V. Riffault, A. Saiz-Lopez, G. Siour, P. Zapf &
731   C. Guieu, ProcEss studies at the Air-sEa Interface after dust deposition in the
732   MEditerranean sea (PEAcEtIME) cruise: Atmospheric and FAST ACTION overview
733   and illustrative observations, in preparation (a) (this special issue)

734   29.   Desboeufs K., C. Giorio, S. Triquet, V. Riffault, P. Chazette, J. Dinasquet, F. Dulac,
735   F. Fu, G. Siour, K. Sellegri, J. Dinasquet, D. García-Nieto, A. Doglioli, P. Formenti,
736   A. Saiz-Lopez, C. Guieu and J.-F. Doussin, New particle formation in the marine

737   boundary layer after wet Saharan dust deposition in the Mediterranean Sea, in

738   preparation (b)

739   30. Desboeufs K., N. Leblond, T. Wagener, E. Bon Nguyen & C. Guieu (2014) Chemical

740   fate and settling of mineral dust in surface seawater after atmospheric deposition

741   observed from dust seeding experiments in large mesocosms, Biogeosciences, 11,

742   5581-5594, doi:10.5194/bg-11-5581-2014.

743   31. Desboeufs, K., Bon Nguyen, E., Chevaillier, S., Triquet, S., & Dulac, F. (2018) Fluxes

744   and sources of nutrient and trace metal atmospheric deposition in the northwestern

745   Mediterranean, Atmospheric Chemistry and Physics, 18, 14477–14492,

746   doi:10.5194/acp-18-14477-2018.

747   32. Desgranges M-M, Petrova1 M.V., Dufour A., Oursel B., Layoun P., Guieu C., Point

748   D., Sarthou G., Jacquet S., Heimbürger-Boavida L-E, Methylmercury: a new tracer for

749   the remineralization of organic matter? in preparation (this special issue)

750   33. Di Iorio, T., di Sarra, A., Sferlazzo, D.M., Cacciani, M., Meloni, D., Monteleone, F.,

751   Fuà, D., & Fiocco, G. (2009) Seasonal evolution of the tropospheric aerosol vertical

752   profile in the central Mediterranean and role of desert dust, Journal of Geophysical

753   Research: Atmospheres, 114, D02201, doi:10.1029/2008JD010593.

754   34. Dinasquet J., Bigeard E., Obernosterer I. & Baudoux A-C., Impact of dust enrichment

755   on the microbial food web under present and future conditions of pH and temperature,

756   in preparation (this special issue)

757   35. Doglioli, A. M., Nencioli, F., Petrenko, A. A., Rougier, G., Fuda, J. L., & Grima, N.

758   (2013) A software package and hardware tools for in situ experiments in a Lagrangian

759   reference frame. Journal of Atmospheric and Oceanic Technology, 30, 1940-1950,

760   doi:10.1175/JTECH-D-12-00183.1.

761   36. d'Ortenzio, F., Iudicone, D., de Boyer Montegut, C., Testor, P., Antoine, D., Marullo,

762   S., Santoleri, R., & Madec, G. (2005) Seasonal variability of the mixed layer depth in

763   the Mediterranean Sea as derived from in situ profiles, Geophysical Research Letters,

764   32, L12605, doi:10.1029/2005GL022463.

765   37. d'Ovidio, F., Della Penna, A., Trull, T. W., Nencioli, F., Pujol, M.-I., Rio, M.-H., Park,

766   Y.-H., Cotté, C., Zhou, M., & Blain, S. (2015) The biogeochemical structuring role of

767   horizontal stirring: Lagrangian perspectives on iron delivery downstream of the

768   Kerguelen Plateau, Biogeosciences, 12, 5567–5581, 2015, doi:10.5194/bg-12-5567-

769   2015.

770   38.   Dulac F., C. Moulin, H. Planquette, M. Schulz, & M. Tartar (2004)

771   African dust deposition and ocean colour in the eastern Mediterranean. Rapp. Comm.

772   Int. Mer Médit., Vol. 37, 190, Commission Internationale pour l'Exploration

773   Scientifique de la Méditerranée, Monaco.

774   39.   Engel, A., Zäncker, B., Michels, J., Liebetrau, V. Interactions between organic matter

775   and aeolian mineral dust in the sea surface microlayer, in preparation

776   40.   Escudero, M., Castillo, S., Querol, X., Avila, A., Alarcón, M.,Viana, M. M., Alastuey,

777   A., Cuevas, E., & Rodríguez, S. (2005) Wet and dry African dust episodes over

778   eastern Spain, J. Geophys. Res., 110, D18S08, doi:10.1029/2004JD004731.

779   41.   Feliu G., Pagano M., & Carlotti C. Structure and functioning of epipelagic

780   mesozooplankton in the Mediterranean sea during spring peacetime cruise 2017, in

781   preparation (this special issue)

782   42.   Formenti, P., D'Anna, B., Flamant, C., Mallet, M., Piketh, S. J., Schepanski, K., ... &

783   Chaboureau, J. P. (2019) The Aerosols, Radiation and Clouds in southern Africa

784   (AEROCLO-sA) field campaign in Namibia: overview, illustrative observations and

785   way forward, Bulletin of the American Meteorological Society, 100, 1277-1298,

786   doi:10.1175/BAMS-D-17-0278.1.

787   43.   Freney E., K. sellegri, A. Nicosia, M. Bloss, E. Asmi, M. Rinaldi, D. Lefevre, M.

788   Thyssen, G. Gregori, K. Desboeufs & C. Guieu, High time resolution measurements

789   of organic content and biological origin of Mediterranean sea spray aerosol (this

790   special issue)

791   44.   Fu F., Desboeufs K., Tovar-Sánchez A., Bressac M., Triquet S., Doussin J-F, Giorio

792   C., Dulac F. & Guieu C., Solubility and concentration of trace metals and nutrients in

793   wet deposition and impact on their marine concentration during PEACETIME cruise

794   in the Mediterranean Sea, in preparation (b) (this special issue)

795   45.   Fu F., Desboeufs K., Triquet S., Doussin J-F, Giorio C., Dulac F. & Guieu C.,

796   Solubility and sources of trace metals and nutrients associated with aerosols collected

797   during cruise PEACETIME in the Mediterranean Sea, in preparation (a) (this special

798   issue)

799   46.   Fu, Y., Desboeufs, K., Vincent, J., Bon Nguyen, E., Laurent, B., Losno, R., & Dulac,

800   F. (2017) Estimating chemical composition of atmospheric deposition fluxes from

801   mineral insoluble particles deposition collected in the western Mediterranean region,

802   Atmospheric Measurement Techniques, 10, 4389–4401, doi:10.5194/amt-10-4389-
803   2017.

804 47. Galletti, Y., S. Becagli, A. di Sarra, M. Gonnelli, E. Pulido-Villena, D.M. Sferlazzo,
805   R. Traversi, S. Vestri, C. Santinelli, Atmospheric deposition of organic matter at a
806   remote site in the 1 Central Mediterranean Sea: implications for marine ecosystem
807   (this special issue)

808 48. Gallisai, R., Peters, F., Volpe, G., Basart, S., & Baldasano, J. M. (2014) Saharan dust
809   deposition may affect phytoplankton growth in the Mediterranean Sea at ecological
810   time scales. PloS ONE, 9, e110762, doi:10.1371/journal.pone.0110762.

811 49. Garcia-Nieto D., N. Benavent, Carlos A. Cuevas & A. Saiz-Lopez, MAXDOAS
812   measurements of trace gases and aerosols over the Mediterranean Sea during the
813   PEACETIME cruise, in preparation (this special issue)

814 50. Garel, M., Bonin, P., Martini, S., Guasco, S., Roumagnac, M., Bhairy, N., ... &
815   Tamburini, C. (2019). Pressure-Retaining Sampler and High-Pressure Systems to
816   Study Deep-Sea Microbes Under in situ Conditions. Frontiers in microbiology, 10,
817   453.

818 51. Gazeau F., Alliouane, S., Stolpe, C., Irisson, J.-O., Marro S., Dolan J., Blasco T., Uitz
819   J., Dimier C., Grisoni J.-M., De Liège G., Hélias-Nunige S., Djaoudi K., Pulido-
820   Villena E., Dinasquet J., Obernosterer I., Ridame C., & Guieu C. Impact of dust
821   enrichment on Mediterranean plankton communities under present and future
822   conditions of pH and temperature : an overview, in preparation (a) (this special issue)

823 52. Gazeau F., Marañon E., Van Wambeke F., Alliouane S., Stolpe C., Blasco T., Ridame
824   C., Pérez-Lorenzo M., Engel A., Zäncker B., & Guieu C. Impact of dust enrichment
825   on carbon budget and metabolism of Mediterranean plankton communities under
826   present and future conditions of pH and temperature, in preparation (b) (this special
827   issue)

828 53. Gitelson A., Karnieli, A., Goldman, N., Yacobi, Y.Z., & Mayo, M. (1996) Chlorophyll
829   estimation in the Southeastern Mediterranean using CZCS images: adaptation of an
830   algorithm and its validation, Journal of Marine Systems, 9, 283-290,
831   doi:10.1016/S0924-7963(95)00047-X.

832 54. Gonzales, L., & Briottet, X (2017) North Africa and Saudi Arabia day/night sandstorm
833   survey (NASCube), Remote Sensing, 9, 896, doi:10.3390/rs9090896.

33

Biogeosciences
Discussions

834 55. Guerzoni, S., Chester, R., Dulac, F., Herut, B., Loÿe-Pilot, M. D., Measures, C.,
835   Migon, C., Molinaroli, E., Moulin, C., Rossini, P., Saydam, C., Soudine, A., & Ziveri,
836   P. (1999) The role of atmospheric deposition in the biogeochemistry of the
837   Mediterranean Sea, Progress in Oceanography, 44, 147-190, doi:10.1016/S0079-
838   6611(99)00024-5.

839 56. Guerzoni, S., Quarantotto, G., Molinaroli, E., & Rampazzo, G. (1995) More data on
840   source signature and seasonal fluxes to the Central Mediterranean Sea of aerosol dust
841   originated in desert areas, in Water Poll. Res. Rep., 32, J.-M. Martin and H. Barth
842   Eds., 253-260.

843 57. Guieu C., Aumont O., Gazeau F., Louis J., Ternon E., Leblond N., Bressac M.,
844   Contribution of the "lithogenic carbon pump" to POC export in the ocean, in
845   preparation

846 58. Guieu C., Ridame, C., Pulido-Villena, E., Bressac, M., Desboeufs, K., & Dulac, F.
847   (2014b) Impact of dust deposition on carbon budget: a tentative assessment from a
848   mesocosm approach, Biogeosciences, 11, 5621-5635, doi:10.5194/bg-11-5621-2014.

849 59. Guieu, C., Aumont, O., Paytan, A., Bopp, L., Law, C.S., Mahowald, N., Achterberg,
850   E.P., Marañón, E., Salihoglu, B., Crise, A., Wagener, T., Herut, B., Desboeufs, K.,
851   Kanakidou, M., Olgun, N., Peters, F., Pulido-Villena, E., Tovar-Sanchez, A,. &
852   Völker, C. (2014a) The significance of episodicity in atmospheric deposition to Low
853   Nutrient Low Chlorophyll regions, Global Biogeochemical Cycles, 2014,
854   doi:10.1002/2014GB004852.

855 60. Guieu, C., Bonnet, S., Wagener, T., & Loÿe-Pilot, M.D. (2005) Biomass burning as a
856   source of dissolved iron to open ocean? Geophysical Research Letters, 32, L19608,
857   doi:10.1029/2005GL022962.

858 61. Guieu, C., Chester, R., Nimmo, M., Martin, J.M., Guerzoni, S., Nicolas, E., Mateu, J.
859   & Keyse, S. (1997) Atmospheric input of dissolved and particulate metals to the
860   northwestern Mediterranean, Deep-Sea Research II, 44, 655-674, doi: 10.1016/S0967-
861   0645(97)88508-6.

862 62. Guieu, C., Loÿe-Pilot, M-D, Benyaya, L., & Dufour, A. (2010) Spatial and temporal
863   variability of atmospheric fluxes of metals (Al, Fe, Cd, Zn and Pb) and phosphorus
864   over the whole Mediterranean from a one-year monitoring experiment;
865   Biogeochemical implications, Marine Chemistry, 120, 164-178,
866   doi:10.1016/j.marchem.2009.02.004.

867   63.   Heimbürger, L.E., Migon, C., Dufour, A., Chiffoleau, J.-F., & Cossa, D. (2010)
868   Decadal trends and evolutions of trace-metals (Al, Cd, Co, Cu, Fe, Mn, Ni, Pb, Zn) in
869   the western Mediterranean atmosphere, Science of the Total Environment, 408, 2629-
870   2638, doi:10.1016/j.scitotenv.2010.02.042.
871   64.   Holben, B.N., Eck, T.F., Slutsker, I., Tanré, D., Buis, J.P., Setzer, A., Vermote, E.,
872   Reagan, J.A., Kaufman, Y.J., Nakajima, T., Lavenu, F., Jankowiak, I., & Smirnov, A.
873   (1998) AERONET—A federated instrument network and data archive for aerosol
874   characterization, Remote Sensing of Environment, 66, 1-16, doi:10.1016/S0034-
875   4257(98)00031-5.
876   65.   Jacquet S, Garel M, Tamburini C, A. Dufour, N. Bhairy, S. Gasco & D. Lefèvre,
877   Particulate biogenic barium and carbon remineralization fluxes at mesopelagic depths
878   during the PEACETIME cruise, in preparation (this special issue)
879   66.   Jordi, A., Basterretxea, G., Tovar-Sánchez, A., Alastuey, A., & Querol, X. (2012)
880   Copper aerosols inhibit phytoplankton growth in the Mediterranean Sea, Proc. of the
881   National Academy of Sciences, 109, 21246-21249, doi: 10.1073/pnas.1207567110.
882   67.   Kallos, G., Spyrou, C., Astitha, M., Mitsakou, C., Solomos, S., Kushta, J., Pytharoulis,
883   I., Katsafados, P., Mavromatidis, E., Papantoniou, N., & Vlastou, G. (2009) Ten-year
884   operational dust forecasting - Recent model development and future plans.
885   WMO/GEO Expert Meeting on an International Sand and Dust Storm Warning
886   System, IOP Conference Series: Earth and Environmental Science, 7, 012012,
887   doi:10.1088/1755-1307/7/1/012012.
888   68.   Kanamitsu, M. (1989) Description of the NMC global data assimilation and forecast
889   system, Weather and Forecasting, 4, 335-342, doi:10.1175/1520-
890   0434(1989)004<0335:DOTNGD>2.0.CO;2.
891   69.   Kouvarakis, G., Mihalopoulos, N., Tselepides, T., & Stavrakakis, S. (2001) On the
892   importance of atmospheric nitrogen inputs on the productivity of eastern
893   Mediterranean, Global Biogeochemical Cycles, 15, 805–818,
894   doi:10.1029/2001GB001399.
895   70.   Kubilay N., S. Nickovic, C. Moulin, & F. Dulac (2000) An illustration of the
896   transport and deposition of mineral aerosol onto the eastern Mediterranean,
897   Atmospheric Environment, 34, 1293-1303, doi:10.1016/S1352-2310(99)00179-X.
898   71.   Law, C.S., Brévière E., de Leeuw, G., Garçon V., Guieu, C., Kieber, D.J.,
899   Kontradowitz, S., Paulmier, A., Quinn, P.K., Saltzman, E.S., Stefels, J., & von

900   Glasow, R. (2013) Evolving Research Directions in Surface Ocean-Lower

901   Atmosphere (SOLAS) Science, Environmental Chemistry, 10, 1-16,

902   doi:10.1071/EN12159.

903   72.   Legrand, M., Plana-Fattori, A., & N'doumé, C. (2001) Satellite detection of dust using

904   the IR imagery of Meteosat: 1. Infrared difference dust index, Journal of Geophysical

905   Research: Atmospheres, 106, 18251-18274, doi:10.1029/2000JD900749.

906   73.   Lionello P., Abrantes, F., Congedi, L., Dulac, F., Gacic, M., Gomiz, D., Goodess, C.,

907   Hoff, H., Kutiel, H., Luterbacher, J., Planton, S., Reale, M., Schröder, K., Struglia,

908   M.V., Toreti, A., Tsimplis, M., Ulbrich, U., & Xoplaki, E. (2012) Introduction:

909   Mediterranean climate−Background information, In The Climate of the Mediterranean

910   Region: From the Past to the Future, P. Lionello Ed., Elsevier, pp. xxxv-xc,

911   doi:10.1016/B978-0-12-416042-2.00012-4.

912   74.   Louis J., Bressac, M., Pedrotti, M.L., & Guieu, C. (2015) Dissolved inorganic nitrogen

913   and phosphorus dynamics in abiotic seawater following an artificial Saharan dust

914   deposition, Frontiers in Marine Sciences, 2, 27, doi:10.3389/fmars.2015.00027.

915   75.   Louis, J., Pedrotti, M. L., Gazeau, F., & Guieu, C. (2017) Experimental evidence of

916   formation of Transparent Exopolymer Particles (TEP) and POC export provoked by

917   dust addition under current and high pCO$_2$ conditions, PloS one, 12, e0171980,

918   doi:10.1371/journal.pone.0171980.

919   76.   Loÿe-Pilot, M. D., Martin, J. M., & Morelli, J. (1986) Influence of Saharan dust on the

920   rain acidity and atmospheric input to the Mediterranean, Nature, 321, 427-428,

921   doi:10.1038/321427a0.

922   77.   Loÿe-Pilot, M.-D., & Martin, J.-M. (1996) Saharan dust input to the western

923   Mediterranean: an eleven years record in Corsica, in The Impact of Desert Dust

924   Across the Mediterranean, S. Guerzoni and R. Chester Eds., Kluwer, 191-199.

925   78.   Mallet, M., Chami, M., Gentili, B., Sempéré, R., & Dubuisson, P. (2009) Impact of

926   sea-surface dust radiative forcing on the oceanic primary production: A 1D modeling

927   approach applied to the West African coastal waters. Geophysical Research Letters,

928   36, L15828, doi:10.1029/2009GL039053.

929   79.   Mallet, M., et al. (2016) Overview of the Chemistry-Aerosol Mediterranean

930   Experiment/Aerosol Direct Radiative Forcing on the Mediterranean Climate

931   (ChArMEx/ADRIMED) summer 2013 campaign, Atmospheric Chemistry and

932   Physics, 16, 455–504, doi:10.5194/acp-16-455-2016.

933 80. Marañón E, Pérez-Lorenzo M, Van Wambeke F, Uitz J, Dinasquet J, Haëntjens N,

934   Dimier C, Deep maxima of phytoplankton biomass, primary production and bacterial

935   production in the Mediterranean sea during late spring, in preparation (this special

936   issue)

937 81. Marconi, M., Sferlazzo, D. M., Becagli, S., Bommarito, C., Calzolai, G., Chiari, M., di

938   Sarra, A., Ghedini, C., Gómez-Amo, J. L., Lucarelli, F., Meloni, D., Monteleone, F.,

939   Nava, S., Pace, G., Piacentino, S., Rugi, F., Severi, M., Traversi, R., & Udisti, R.

940   (2014) Saharan dust aerosol over the central Mediterranean Sea: PM_{10} chemical

941   composition and concentration versus optical columnar measurements, Atmospheric

942   Chemistry and Physics, 14, 2039-2054, https://doi.org/10.5194/acp-14-2039-2014.

943 82. Markaki, Z., Loÿe-Pilot, M. D., Violaki, K., Benyahya, L., & Mihalopoulos, N. (2010)

944   Variability of atmospheric deposition of dissolved nitrogen and phosphorus in the

945   Mediterranean and possible link to the anomalous seawater N/P ratio, Marine

946   Chemistry, 120, 187-194, doi:10.1016/j.marchem.2008.10.005.

947 83. Markaki, Z., Oikonomou, K., Kocak, M., Kouvarakis, G., Chaniotaki, A., Kubilay, N.,

948   & Mihalopoulos, N. (2003) Atmospheric deposition of inorganic phosphorus in the

949   Levantine Basin, eastern Mediterranean: Spatial, temporal variability, and its role in

950   seawater productivity, Limnology and Oceanography, 48, 1557–1568,

951   doi:10.4319/lo.2003.48.4.1557.

952 84. Meloni, D., di Sarra, A., Biavati, G., DeLuisi, J.J., Monteleone, F., Pace, G.,

953   Piacentino, S., & Sferlazo, D.M. (2007) Seasonal behavior of Saharan dust events at

954   the Mediterranean island of Lampedusa in the period 1999–2005, Atmospheric

955   Environment, 41, 3041-3056, doi:10.1016/j.atmosenv.2006.12.001.

956 85. Menna, M., Poulain, P. M., Ciani, D., Doglioli, A., Notarstefano, G., Gerin, R., ... &

957   Drago, A. (2019). New insights of the Sicily Channel and southern Tyrrhenian Sea

958   variability. Water, 11(7), 1355.

959 86. Moon, J. Y., Lee, K., Tanhua, T., Kress, N., and Kim, I. N.: Temporal nutrient

960   dynamics in the Mediterranean Sea in response to anthropogenic inputs, Geophysical

961   Research Letters, 43, 5243–5251, doi:10.1002/2016GL068788, 2016.

962 87. Morales-Baquero, R., & Pérez-Martínez, C. (2016) Saharan versus local influence on

963   atmospheric aerosol deposition in the southern Iberian Peninsula: Significance for N

964   and P inputs, Global Biogeochemical Cycles, 30, 501-513, doi:

965   10.1002/2015GB005254.

Biogeosciences
Discussions

966   88.   Moulin, C., Lambert, C. E., Dayan, U., Masson, V., Ramonet, M., Bousquet, P.,
967   Legrand, M., Balkanski, Y.J., Guelle, W., Marticorena, B., Bergametti, G., & Dulac,
968   F. (1998) Satellite climatology of African dust transport in the Mediterranean
969   atmosphere. Journal of Geophysical Research: Atmospheres, 103, 13137-13144,
970   doi:10.1029/98JD00171.

971   89.   Moutin, T., Doglioli, A. M., De Verneil, A., & Bonnet, S. (2017) Preface: The
972   Oligotrophy to the UlTra-oligotrophy PACific Experiment (OUTPACE cruise, 18
973   February to 3 April 2015), doi:10.5194/bg-14-3207-2017.

974   90.   Nabat, P., Somot, S., Mallet, M., Michou, M., Sevault, F., Driouech F., Meloni, D., Di
975   Sarra, A., Di Biagio, C., Formenti, P., Sicard, M., Léon, J.-F. and Bouin, M.-N.
976   (2015), Dust aerosol radiative effects during summer 2012 simulated with a coupled
977   regional aerosol-atmosphere-ocean model over the Mediterranean region, *Atm. Chem.*
978   *Phys.*, 15, 3303-3326, doi:10.5194/acp-15-3303-2015.

979   91.   Nencioli, F., d'Ovidio, F., Doglioli, A. M., & Petrenko, A. A. (2011) Surface coastal
980   circulation patterns by in-situ detection of Lagrangian coherent structures,
981   Geophysical Research Letters, 38, L17604, doi:10.1029/2011GL048815.

982   92.   Pérez, C., Haustein, K. Janjic, Z. Jorba, O., Huneeus, N., Baldasano, J.M., Black, T.,
983   Basart, S., Nickovic, S., Miller, R.L., Perlwitz, J.P., Schulz, M., & Thomson, M.
984   (2011) Atmospheric dust modeling from meso to global scales with the online
985   NMMB/BSC-Dust model - Part 1: Model description, annual simulations and
986   evaluation, Atmospheric Chemistry and Physics, 11, 13001-13027, doi:10.5194/acp-
987   11-13001-2011.

988   93.   Petrenko, A.A., Doglioli AM, Nencioli F., Kersalé M., Hu Z., & d'Ovidio F. (2017) A
989   review of the LATEX project: mesoscale to submesoscale processes in a coastal
990   environment, Ocean Dynamics, 67, 513-533, doi:10.1007/s10236-017-1040-9.

991   94.   Pey, J., Querol, X., Alastuey, A., Forastiere, F., & Stafoggia, M. (2013) African dust
992   outbreaks over the Mediterranean Basin during 2001–2011: PM_{10} concentrations,
993   phenomenology and trends, and its relation with synoptic and mesoscale meteorology.
994   Atmospheric Chemistry and Physics, 13, 1395-1410, doi:10.5194/acp-13-1395-2013.

995   95.   Pitta, P., Kanakidou, M., Mihalopoulos, N., Christodoulaki, S., Dimitriou, P. D.,
996   Frangoulis, C., Giannakourou, A., Kagiorgi, M., Lagaria, A., Nikolaou, P.,
997   Papageorgiou, N., Psarra, S., Santi, I, Tsapakis, M., Tsiola, A., Viollaki, K., &
998   Petihakis, G. (2017) Saharan dust deposition effects on the microbial food web in the

999   Eastern Mediterranean: a study based on a mesocosm experiment. Frontiers in Marine

1000   Science, 4, 117, doi:10.3389/fmars.2017.00117.

1001 96.   Pulido-Villena E., A.-C. Baudoux, I. Obernosterer, M. Landa, J. Caparros, P. Catala,

1002   C. Georges, J. Harmand, & C. Guieu (2014) Microbial food web dynamics in response

1003   to a Saharan dust event: results from a mesocosm study in the oligotrophic

1004   Mediterranean Sea, Biogeosciences, 11, 5607–5619, doi:10.5194/bg-11-5607-2014.

1005 97.   Pulido-Villena, E., Van Wambeke, F., Desboeufs, K., Petrenko, A., Barrillon, S.,

1006   Djaoudi, K., Doglioli, A., D'Ortenzio, F., Estournel, C., Fu, Y., Gaillard, T., Guasco,

1007   S., Marsaleix, P., Nunige, S., Raimbault, P., Taillandier, V., Triquet, S. & Guieu, C.,

1008   Relative contribution of internal vs. external sources of phosphate to the surface mixed

1009   layer in the P-depleted Mediterranean Sea (Peacetime cruise), in preparation (this

1010   special issue)

1011 98.   Reygondeau, G., Irisson, J.-O., Ayata, S., Gasparini, S., Benedetti, F., Albouy, C.,

1012   Hattab, T., Guieu, C., Koubbi, P. (2014) Definition of the Mediterranean eco-regions

1013   and maps of potential pressures in these eco-regions. Technical Report. Deliverable

1014   Nr. 1.6. FP7-PERSEUS project.

1015 99.   Richon, C., Dutay, J.-C., Dulac, F., Wang, R., & Balkanski, Y (2018b) Modeling the

1016   biogeochemical impact of atmospheric phosphate deposition from desert dust and

1017   combustion sources to the Mediterranean Sea, Biogeosciences, 15, 2499–2524,

1018   https://doi.org/10.5194/bg-15-2499-2018.

1019 100. Richon, C., J.-C. Dutay, F. Dulac, R. Wang, Y. Balkanski, P. Nabat, O. Aumont, K.

1020   Desboeufs, B. Laurent, C. Guieu, P. Raimbault, & J. Beuvier (2018a) Modeling the

1021   impacts of atmospheric deposition of nitrogen and desert dust-derived phosphorus on

1022   nutrients and biological budgets of the Mediterranean Sea, Progress in Oceanography,

1023   163, 21-39, doi:10.1016/j.pocean.2017.04.009.

1024 101. Ridame C., Bigeard E., Dinasquet J., Tovar-Sanchez A., Baudoux A-C., Gazeau F. &

1025   Guieu C., Impact of dust enrichment on N_2 fixation and diversity of diazotrophs under

1026   present and future conditions of pH and temperature, in preparation (this special issue)

1027 102. Ridame, C. , M. Le Moal, C. Guieu, E. Ternon, I. C. Biegala, S. L'Helguen, & M.

1028   Pujo-Pay (2011) Nutrient control of N2 fixation in the oligotrophic Mediterranean Sea

1029   and the impact of Saharan dust events, Biogeosciences, 8, 2773-2783, doi:10.5194/bg-

1030   8-2773-2011.

1031   103.   Ridame, C., Guieu, C. & S. L'Helguen (2013) Strong stimulation of N_2 fixation in

1032   oligotrophic Mediterranean Sea: results from dust addition in large in situ mesocosms,

1033   Biogeosciences, 10, 7333–7346, doi: 10.5194/bg-10-7333-2013.

1034   104.   Riffault V., C. Giorio, K. Desboeufs, J.-F. Doussin, F. Dulac, A. Féron, P. Formenti,

1035   F. Maisonneuve, E. Tison, S. Triquet, P. Zapf, Chemical characterization of gases and

1036   fine aerosols in air masses influenced by ship plumes during the PEACETIME cruise

1037   in the West Mediterranean basin, in preparation (this special issue)

1038   105.   Rolph, G., Stein, A., & Stunder, B. (2017) Real-time Environmental Applications and

1039   Display sYstem: READY, Environmental Modelling & Software, 95, 210-228,

1040   doi:10.1016/j.envsoft.2017.06.025.

1041   106.   Rousselet, L., Doglioli, A. M., de deVerneil, A., Pietri, A., Della Penna, A., Berline,

1042   L., Marrec, P., Grégori, G., Thyssen, M., Carlotti, F., Barrillon, S., Simon-Bot, F.,

1043   Bonal, M., D'Ovidio, F., & Petrenko, A. (2019) Vertical motions and their effects on a

1044   biogeochemical tracer in a cyclonic structure finely observed in the Ligurian Sea,

1045   Journal of Geophysical Research: Oceans, 124, 3561-3574, doi:

1046   10.1029/2018JC014392.

1047   107.   Roy-Barman M., Foliot L., Douville E., Guieu C., Leblond N., Gazeau F., Bressac M.,

1048   Wagener T., & Ridame C., Contrasted release of insoluble elements (Fe, Al, REE, Th,

1049   Pa) during dust deposition in seawater: a minicosm approach, in preparation (this

1050   special issue)

1051   108.   Sciare, J., Bardouki, H., Moulin, C., & Mihalopoulos, N. (2003) Aerosol sources and

1052   their contribution to the chemical composition of aerosols in the Eastern

1053   Mediterranean Sea during summertime. Atmospheric Chemistry and Physics, 3, 291-

1054   302, doi:10.5194/acp-3-291-2003.

1055   109.   Seity, Y., Brousseau, P., Malardel, S., Hello, G., Bénard, P., Bouttier,F., Lac, C., and

1056   Masson, V.: The AROME-France Convective-Scale Operational Model, Mon.

1057   Weather Rev., 139, 976–991,https://doi.org/10.1175/2010MWR3425.1, 2011

1058   110.   Sellegri K., Nicosia A., Freney E., Uitz J., Thyssen M., Grégori G., , Engel A.,

1059   Zäncker B., Haëntjens N., Mas S., Picard D., Saint-Macary A., Peltola M., Rose C.,

1060   Trueblood J., Lefevre D., D'Anna B., Desboeufs K., Meskhidze N., Guieu C. and Law

1061   C., Linking living microorganisms of the Ocean and atmospheric Cloud Condensation

1062   Nuclei production, Science, submitted, 2020

1063   111.   SOLAS 2015-2025: Science Plan and Organisation (2015) SOLAS Scientific Steering
1064   Committee and Emilie Brévière (Editors) SOLAS International Project Office, Kiel.
1065   68 pp.

1066   112.   Spyrou, C., Mitsakou, C., Kallos, G., Louka, P., & Vlastou, G. (2010) An improved
1067   limited area model for describing the dust cycle in the atmosphere, Journal of
1068   Geophysical Research: Atmospheres, 115, D17211, doi:10.1029/2009JD013682.

1069   113.   Stein, A.F., Draxler, R.R, Rolph, G.D., Stunder, B.J.B., Cohen, M.D., & Ngan, F.
1070   (2015) NOAA's HYSPLIT atmospheric transport and dispersion modeling system,
1071   Bull. Amer. Meteor. Soc., 96, 2059-2077, doi:10.1175/BAMS-D-14-00110.1.

1072   114.   Taillandier V., Prieur L. D'Ortenzio F., Ribera d'Alcalà M., and Pulido-Villena E.,
1073   Profiling float observation of thermohaline staircases in the western Mediterranean
1074   Sea and impact on nutrient fluxes, Biogeosciences Discuss.,
1075   https://doi.org/10.5194/bg-2019-504, 2020

1076   115.   Ternon E. , Guieu, C., Loÿe-Pilot, M-D., Leblond, N., Bosc, E., Gasser, B., Martin, J.,
1077   & Miquel, J.-C. (2010) The impact of Saharan dust on the particulate export in the
1078   water column of the North Western Mediterranean Sea, Biogeosciences, 7, 809-826,
1079   doi: 10.5194/bg-7-809-2010.

1080   116.   Ternon E., Guieu, C., Ridame, C., L'Helguen, S, & Catala, P. (2011) Longitudinal
1081   variability of the biogeochemical role of Mediterranean aerosols in the Mediterranean
1082   Sea, Biogeosciences, 8, 1067–1080, doi: 10.5194/bg-8-1067-2011.

1083   117.   Testor P., Send, U., Gascard, J.-C., Millot, C., Taupier-Letage, I., & Béranger, K.
1084   (2005) The mean circulation of the southwestern Mediterranean Sea: Algerian Gyres,
1085   Journal of Geophysical Research, 110, C110017, doi:10.1029/2004JC002861.

1086   118.   The MERMEX Group (2011) Marine ecosystems' responses to climatic and
1087   anthropogenic forcings in the Mediterranean, Progress in Oceanography, 91, 97-166,
1088   doi:10.1016/j.pocean.2011.02.003.

1089   119.   Theodosi, C., Markaki, Z., Tselepides, A., & Mihalopoulos, N. (2010) The
1090   significance of atmospheric inputs of soluble and particulate major and trace metals to
1091   the eastern Mediterranean seawater, Marine Chemistry, 120, 154-163, doi:
1092   10.1016/j.marchem.2010.02.003.

1093   120.   Thieuleux, F., Moulin, C., Bréon, F. M., Maignan, F., Poitou, J., & Tanré, D. (2005)
1094   Remote sensing of aerosols over the oceans using MSG/SEVIRI imagery, Annales
1095   Geophysicae, 23, 3561–3568, doi:10.5194/angeo-23-3561-2005.

Discussions

1096 121. Tovar-Sánchez A., A Rodríguez-Romero, A Engel, B Zäncker, F Fu, E Marañón, M
1097   Pérez-Lorenzo, M Bressac, T Wagener*, K Desboeuf, S Triquet, G Siour, C Guieu,
1098   Characterising the surface microlayer in the Mediterranean Sea: trace metals
1099   concentration and microbial plankton abundance, Biogeosciences Discuss.,
1100   https://doi.org/10.5194/bg-2019-290, 2019
1101 122. Tovar-Sánchez, A., Arrieta, J.M., Duarte, C.M., & Sañudo-Wilhelmy, S.A. (2014)
1102   Spatial gradients in trace metal concentrations in the surface microlayer of the
1103   Mediterranean Sea, Frontiers in Marine Science, 1, 79, doi:
1104   10.3389/fmars.2014.00079.
1105 123. Trueblood J., Nicosia, A., K. sellegri, E. Freney, B. Zäncker, A. Engel, D. Lefevre, M.
1106   Thyssen, G. Gregori, P. Amato, K. Desboeufs and C. Guieu, On the biological origin
1107   of the Ice Nuclei properties of primary marine emissions from the Mediterranean Sea,
1108   in preparation (this special issue)
1109 124. Tsagaraki, T. M., Herut, B., Rahav, E., Berman Frank, I. R., Tsiola, A., Tsapakis, M.;
1110   Giannakourou, A., Gogou, A., Panagiotopoulos, C., Violaki, K.; et al. Atmospheric
1111   Deposition Effects on Plankton Communities in the Eastern Mediterranean: A
1112   Mesocosm Experimental Approach, Frontiers in Marine Science 2017, 4, 210.
1113   https://doi.org/10.3389/fmars.2017.00210.
1114 125. Tsapakis, M., Apsotolaki, M., Eisenreich, S., & Stephanou, E.G. (2006) Atmospheric
1115   deposition and marine sedimentation fluxes of polycyclic aromatic hydrocarbons in
1116   the Eastern Mediterranean Basin. Environmental Science and Technology 40, 4922-
1117   4927.
1118 126. Van Wambeke F., Pulido-Villena E., Djaoudi K., Garel M., Guasco S., Helias S.,
1119   Dinasquet J., Tallandier V. & Tamburini C., Spatial patterns of biphasic
1120   ectoenzymatic kinetics in link with biogeochemical properties within surface, deep
1121   chlorophyll maximum layer, levantine intermediate waters and deep waters in the
1122   Mediterranean Sea in spring, in preparation (this special issue)
1123 127. Varga, G., Újvári, G., & Kovács, J. (2014) Spatiotemporal patterns of Saharan dust
1124   outbreaks in the Mediterranean Basin, Aeolian Research, 15, 151-160,
1125   doi:10.1016/j.aeolia.2014.06.005.
1126 128. Vincent, J., Laurent, B., Losno, R., Bon Nguyen, E., Roullet, P., Sauvage, S.,
1127   Chevaillier, S., Coddeville, P., Ouboulmane, N., di Sarra, A. G., Tovar-Sánchez, A.,
1128   Sferlazzo, D., Massanet, A., Triquet, S., Morales Baquero, R., Fornier, M., Coursier,

1129   C., Desboeufs, K., Dulac, F., & Bergametti, G. (2016) Variability of mineral dust
1130   deposition in the western Mediterranean basin and south-east of France, Atmospheric
1131   Chemistry and Physics, 16, 8749-8766, doi:10.5194/acp-16-8749-2016.

1132 129. Violaki K., Zarbas, P., & Mihalopoulos, N. (2010) Long-term measurements of water-
1133   soluble organic nitrogen (WSON) in atmospheric deposition in the Eastern
1134   Mediterranean: Fluxes, origin and biogeochemical implications, Marine Chemistry,
1135   120, 179–186, doi:10.1016/j.marchem.2009.08.004.

1136 130. Wagener, T., Guieu C., & Leblond N. (2010) Effects of dust deposition on iron cycle
1137   in the surface Mediterranean Sea: results from a mesocosm seeding experiment,
1138   Biogeosciences, 7, 3769-3781, doi: 10.5194/bg-7-3769-2010.

1139 131. Wuttig K., Wagener, T., Bressac, M., Dammshäuser, A., Streu, P., Guieu, C., &
1140   Croot, P.L. (2013) Impacts of dust deposition on dissolved trace metal concentrations
1141   (Mn, Al and Fe) during a mesocosm experiment, Biogeosciences 10, 2583-2600,
1142   doi:10.5194/bg-10-2583-2013.

1143 132. Yang, F., Pan, H.-L., Krueger, S.K., Moorthi, S., & Lord, S.J. (2006) Evaluation of the
1144   NCEP global forecast system at the ARM SGP site, Monthly Weather Review, 134,
1145   3668-3690, doi:10.1175/MWR3264.1.

1146 133. Zhang, J., Reid, J.S., Westphal, D.L., Baker, N.L., & Hyer, E.J. (2008) A system for
1147   operational aerosol optical depth data assimilation over global oceans, Journal of
1148   Geophysical Research: Atmospheres, 113, D10208, doi:10.1029/2007JD009065.

1149

1150

1151 **Table 1.** Date of occupation, position and depth of the short stations (ST1-ST10), of the long

1152 stations (TYRR, ION, FAST) and of the SAV station.

	arrival date	local time	departure date	local time	depth m	lat N	long E
ST1	12/05/2017	05:45	12/05/2017	21:15	1580	41°53.5	6°20
ST2	13/05/2017	06:30	13/05/2017	13:08	2830	40°30.36	6°43.78
ST3	14/05/2017	06:00	14/05/2017	13:30	1404	39°08.0	7°41.0
ST4	15/05/2017	05:56	15/05/2017	13:04	2770	37°59.0	7°58.6
ST5	16/05/2017	04:00	16/05/2017	10:58	2366	38°57.2	11°1.4
TYRR	17/05/2017	05:08	21/05/2017	15:59	3395	39°20.4	12°35.56
ST6	22/05/2017	04:50	22/05/2017	10:38	2275	38°48.47	14°29.97
SAV	23/05/2017	11:30	23/05/2017	14:17	2945	37°50.4	17°36.4
ST7	23/05/2017	21:10	24/05/2017	07:15	3627	36°39.5	18°09.3
ION	24/05/2017	18:02	29/05/2017	08:25	3054	35°29.1	19°47.77
ST8	30/05/2017	03:53	30/05/2017	09:41	3314	36°12.6	16°37.5
ST9	01/06/2017	19:13	02/06/2017	04:41	2837	38°08.1	5°50.5
FAST	02/06/2017	20:24	07/06/2017	23:25	2775	37°56.8	2°54.6
ST10	08/06/2017	05:12	08/06/2017	10:25	2770	37°27.58	1°34.0
FAST -bis	08/06/2017	21:06	09/06/2017	00:16	2775	37°56.8	2°55.0

1153

1154

1155 **Table 2. Work at sea during the PEACETIME Cruise and associated publications**

total number	Operations at sea	details	SHORT STATIONS 1–10, SAV		LONG STATIONS TYR	ION	FAST	Papers presenting the data
continuous	Atmospheric sampling	[1]	CONTINUOUS		CONTINUOUS			Desboeufs et al., in prep (a), Desboeufs et al., in prep (b); Fu et al., in prep. (a); Garcia-Nieto et al., in prep.; Riffault et al., in prep.
3	Rain water collection	[2]					x	Fu et al., in prep (b)
continuous	Continuous surface seawater pumping (-5 m)	[3]	CONTINUOUS			x		Freney et al., in prep.; Sellegri et al., submitted; Trueblood et al., in prep.
3 times	Surface seawater pumping (large volume (1800 L) for experiments in Climate Reactors)	[4]			x	x	x	Gazeau et al., in prep (a & b); Ridame et al., in prep.; Roy-Barman et al., in prep.; Dinasquet et al., in prep.; Guieu et al., in prep.
90 casts	Classical Rosette with 24 Niskin bottles or 22 Niskin bottles + 3 HP bottles [1].	[5]	0-500 and 0-bottom					Taillandier et al., submitted; van Wambeke et al., in prep.; Maranon et al., in prep.; Berline et al., in prep.; Jacquet et al., in prep.; Zancker et al., in prep.; Barbieux et al., in prep.; Baumas et al., in prep. Guieu et al., this paper ; Garel et al., 2019
27 casts	Trace metal Clean Rosette on kevlar cable with 24 teflon-coated GoFlo bottles [2].	[6]	0-bottom					Bressac et al., in prep.; Pulido-Villena et al., in prep.; Desgranges et al., in prep., Ridame et al., in prep.
17 sampling	Microlayer sampling (rubber boat)	[7]	x ... SAV: x		xx	xx	xxxx	Tovar-Sanchez et al., in rev.; Zancker et al., in prep.; Engel et al., in prep.
17 free-fall profiles	Optical measurements: HyperPro [3]	[8]	x x x x x x x ; SAV: x		xxxx	xx	xxxx	
23 net tows	Zooplankton Net (0-200 m)	[9]	x x x x x x x x x x		xxxx	xxxxxx	xxxxx	Feliu et al., in prep.
13	Marine snow catcher (depth m)	[10]			70-80 -90- 200	80-100 -150- 200	70-75 - 80-100	

Table 2 (continued)

3 times	Drifting mooring	[11]	x	x	x	Bressac et al., (2019); Bressac et al., in prep.
3 times	Sediment Cores	[12]	x	x	x	Brandt et al., submitted; Brandt et al., in prep.
20 drifters	SVP (Surface Velocity Program) drifters	[13]	x	x		Menna et al., 2019. Guieu et al., this paper; Berline et al.in prep., Desboeufs et al., in prep. (b)
a total of 1000 profiles (0-300m)	Moving Vessel Profiler (begining and end long stations)	[14]	between the short stations and in the long stations area as frequent as possible			Guieu et al., this paper; Berline et al. in prep.
2 deployments, 1 recovery	Biogeochemical ARGO float	[15]		x		Barbieux et al., in prep. ; Taillandier et al., submitted

1] Atmospheric sampling was carried out throughout the transect using PEGASUS dedicated mobile platform (PortablE Gas and Aerosol Sampling UnitS, Formenti et al., 2019) to monitor continuous air gaseous composition (NOx, SO_2, O_3, CO_2, CO, VOC), physico-chemical properties of aerosol particles (mass and number concentration, size-distribution, chemical composition and nutrients contents), parameters of atmospheric dynamics such as the boundary layer, and radiative parameters (incident radiation, optical thickness, optical properties of the particles).

2] Rain sampling of two events that occurred during the cruise. The on-line filtration collector was used to determine the dissolved and particulate composition of rain, including major and trace metals (Al, Ba, Cd, Co, Cr, Cu, Fe, Mo, Mn, Ni, Pb, Sr, Ti, V, Zn), atmospheric inorganic compounds (sulfate, chlorure, Na, Mg, K, Ca...) and dissolved nutrients (phosphate, nitrate, ammonium).

3] An innovative system of continuous "clean" pumping activated by a large peristaltic pump connected to a tube plunged at 5 m under the surface seawater inside a TraOcean was set up. The water was conveyed in a dedicated laboratory and distributed to several instruments to assess its

Biogeosciences
Discussions

Open Access

EGU

1166 chemical properties (carbonate chemistry, O_2), microbial assemblages, hydrological properties, optical properties related to community and particle

1167 composition and aerosol production (chemical composition, particles spectrum) throughout the transect.

1168 [4] Climate reactor experiments: 6 large volume tanks (300 L) were filled with surface water. After artificial dust seeding at the surface of 4 of the

1169 reactors, the impact of dust deposition on biogeochemical stocks and fluxes under present and future environmental conditions (acidification and

1170 increase of the temperature of the sea water) was followed during 4 days (TYR and ION) and 5 days (FAST). [listing all parameters measured: see

1171 Table 1, Gazeau et al., this issue (a)].

1172 [5] The "classical" Rosette was composed of a CTD underwater unit that continuously collected the following parameters: pressure, temperature

1173 and salinity of seawater, dissolved oxygen concentration, photosynthetically active radiation (PAR), beam transmission (at 650 nm), chlorophyll-

1174 a fluorescence. A LISST (Laser *in situ* Scattering and Transmissiometry Deep (LISST-Deep), Sequoia Sc) was mounted independently on the CTD

1175 frame. This instrumental package was also composed of a sampling system : 24 12-L Niskin bottles could be fired at specified levels during upcasts.

1176 Some Niskin could be replaced by High Pressure (HP) bottles that allowed hyperbaric sampling on dedicated deep casts. Water from the classical

1177 Rosette was used to quantify O_2, AT/CT, nutrients, DOC, POC/PON, hyperspectral particulate absorption coefficient, hyperspectral CDOM

1178 absorption coefficient, chlorophyll pigments, viruses abundance and lysogeny, bacteria, flagellates and pico-nanoeukaryotes abundance (by

1179 cytometry), total combined carbohydrates, total hydrolysable amino acids, gel particles (TEP and CSP), bacterial production, dissolved and

1180 particulate primary production, virus diversity, and eukaryote diversity.

1181 [6] The trace metal "clean" Rosette was composed of a titanium CTD underwater unit that continuously collected the following parameters:

1182 pressure, temperature and salinity of seawater, dissolved oxygen concentration, CDOM Fluorescence. This instrumental package was also

1183 composed of a teflon-coated sampling system: 24 GoFlo bottles could be fired at specified levels during upcast. Water from the clean rosette was

1184 used to measure dissolved metals (Al, Cd, Co, Cu, Fe, Mo, Ni, Pb, V, Zn) and particulate (Al, Ba, Ca, Cu, Fe, Mn, Ni, Ti, Zn), total mercury,

1185 methyl mercury, inorganic phosphate and nitrate (nano-molar), nutrients (to be measured with Technicon), di-nitrogen fixation, diazotrophs

1186 diversity (only at Station 10).

1187 [7] Discrete sampling of the surface micro layer (SML) was performed from a rubber boat using gas plate systems. Dissolved (<0.22 μm) and total

1188 (unfiltered) SML samples were collected for trace metals (Cd, Co, Cu, Fe, Ni, Mo, V, Zn and Pb) and nutrients analysis. Same metals were also

1189 measured in a subsurface (0-1 m) filtered (0.22 μm) sample. Samples were collected for the determination of total combined carbohydrates, total

1190 hydrolysable amino acids, gel particles (TEP and CSP). DNA was extracted from filters from the surface microlayer and subsurface water (~ 20

1191 cm). Three experimental SML additions were carried out in waters of TYR, ION and FAST stations.

1192 [8] The HyperPro measured hyperspectral upwelling radiance (Lu) and downwelling irradiance (Ed) at the daily solar maximum.

1193 [9] Samples collected by net hauls between 0 and 300 m performed with a BONGA net equipped with a 100 μm and a 200 μm mesh size.

1194 Zooplankton abundance, biomass and taxonomy were obtained in 3 size classes: <200 μm; >200 - <1000 μm and >1000 μm. At long stations,

1195 additional samples were taken for stable isotopes analyses.

48

1196 [10] The large Marine Snow Catcher bottle (100 L) was used at long duration stations to collect suspended particles, slow sinking particles and fast

1197 sinking particles. Heterotrophic production of prokaryotes attached to these different particles types was measured along with TEP abundance and

1198 POC concentrations. In addition concentration kinetics of aminopeptidase, alkaline phosphatase and beta D glucosidase was measured. Diversity

1199 of microorganisms collected in each type of particles was analyzed by barcoding and sequencing.

1200 [11] The mooring was equipped with (i) 3 Technicap type PPS5 particle traps at 200, 500 and 1000 m, each equipped with inclinometers, (ii) 3

1201 IODA (In Situ Oxygen Dynamics Auto-analyzer) at 5, 90 and 200 m; (iii) 2 in situ particle interceptor/incubator – RESPIRE (at 120 m and 200

1202 m), (iv) 2 trace metal clean RESPIRE (at 110 m and 190 m), and (v) 1 Sediment Trap Station with 4, ø80-mm tubes in transparent PVC. The line

1203 was also equipped with 4 CTD / O2 type SeaBird Microcat SBE37, 4 Aquadopp Doppler current meter from Nortek brand, 5 RBR Autonomous

1204 Temperature and Pressure Sensors, 5 RBR Autonomous Temperature Sensors alone. Drifting moorings were deployed for 4 days at TYR and ION

1205 and 5 days at FAST. Fluxes for particulate mass, carbon, organic carbon, inorganic carbon, nitrogen, calcium, aluminium, iron, biogenic and

1206 lithogenic silica were determined from PPS5 samples.

1207 [12] At TYR (depth 3395 m), ION (depth 3054 m) and FAST (2775 m), sediment core sampling were carried out with a multicorer, sliced into

1208 depth layers to perform DNA extractions.

1209 [13] A total of 20 SVP (Surface Velocity Program) drifters were deployed at the long duration stations to provide information on the current at 15-

1210 m depth.

49

1211   [14] A MVP (Moving Vessel Profiler) was deployed to perform high frequency 0-300 m profiles of CTD (and fluorescence and LOPC-Laser

1212   Optical Particle Counter, when the "big fish" was towed instead of the "small fish") between the short stations and in the long station areas as

1213   frequently as possible (see Figure 12). A total of more than 1000 profiles have been obtained.

1214   [15] Two Biogeochemical Argo profiling floats have been deployed in the Ionian Sea. In addition to the CTD, the floats interfaced bio-optical

1215   sensors that measured fluorescence of Chlorophyll and CDOM, particulate backscattering (700 nm), Photosynthetically Active Radiation and

1216   downwelling irradiance at three wavelengths (380, 412, 490 nm). In addition, the float released at the ION station included an optode that measures

1217   dissolved oxygen and a beam transmissometer (650 nm).

1218

1219

1220 **Figure Captions.**

1221 **Figure 1**. Mediterranean surface mixed layer depth (m) monthly climatology over 1940-2004

1222 (in m; from D'Ortenzio et al., 2005; Copyright 2005 by the American Geophysical Union).

1223 **Figure 2**. Monthly-averaged dust optical depth at 550 nm (1979-2013 period) over the

1224 Mediterranean region from the CNRM-RCSM5 regional coupled climate system model (after

1225 Nabat et al., 2015).

1226 **Figure 3**. Monthly averaged chlorophyll maps derived from SeaWiFS data for the year 1999

1227 (Bosc et al., 2004; Copyright 2004 by the American Geophysical Union).

1228 **Figure 4.** Spatial distribution of the Mediterranean epipelagic marine ecosystems of the

1229 Mediterranean Sea (from Reygondeau et al. 2014). The consensus regions (in white, from Ayata

1230 et al., 2018) from eight regionalisations of the Mediterranean Sea, are characterised by well

1231 defined, relatively homogeneous biogeochemical and hydrodynamical conditions, with similar

1232 temporal dynamics). The transect initially planned is superimposed.

1233 **Figure 5**. Transect of the PEACETIME Cruise: Initial (dotted line) and final track (continuous

1234 line); stations are indicated by filled circles (planned stations: smaller, pink: realized: larger,

1235 orange). The 10 short stations are numbered from St.1 to St.10. TYR, ION, and FAST indicate

1236 the 3 long stations. The SAV station was only performed for the retrieval and launch of floats.

1237 The land-based Lampedusa observatory (purple triangle) and 15 AERONET stations operated

1238 during the cruise are also represented (brown diamonds).

1239 **Figure 6**. Aerosol optical depth at 550 nm derived from MSG/SEVIRI on 3 June 2017; left:

1240 from the 15-mn image acquired at 13:00 UT; right: daily average from 52 images acquired

1241 between 4 and 18:30 UT. The black circle indicates the position of the ship (station FAST) .

1242 The dark grey mask corresponds to land and coastal ocean pixels, the light grey, to cloudy

1243 pixels.

1244 **Figure 7.** NASCube image window over North Africa and southern Europe for 1 June 2017,

1245 02 UT. This nighttime image is derived from MSG/SEVIRI thermal infrared channels by

1246 comparison to a clear reference image for the period, allowing detecting high dust load over the

1247 continental surfaces (Legrand et al., 2001). White tones indicate clouds, the highest being the

1248 brightest and the thermal anomalies attributable to dust are coloured by increasing intensity

1249 from blue to pink. They are associated with increasing AOD from light blue (typically <0.3) to

1250 purple (~1) and pink (>2) (Gonzalez and Briottet, 2017).

1251 **Figure 8.** Rain-lightning-clouds (RLC) image window over the western Mediterranean and

1252 Spanish Peninsula showing clouds (white areas), estimated precipitation (blue shades), and

1253 lightning strikes (yellow circles) obtained by combining SEVIRI infrared images and European

1254 rain radars (from meteoradar.co.uk; access 3 June 2017).

1255 **Figure 9.** Maps of 6-h accumulated desert dust wet deposition fluxes in the western

1256 Mediterranean produced by the forecast run of 2 June 2017 of the three dust transport models

1257 NNMB-BSC-Dust-v2 (top) BSC-DREAM8b (middle) and SKIRON (bottom), at times 3 Jun,

1258 12 UTC and 18 UTC, 4 Jun 18 UTC and 5 Jun 00 UTC from left to right, respectively.

1259 **Figure 10.** Map of the FSLE (Finite Size Lyapunov Exposant, day^{-1}) calculated from the near-

1260 real-time altimetry-derived surface currents for June 4, 2017. The figure is taken from the

1261 SPASSO bulletin of June 5, 2017 with the planned stations shown in black and the route toward

1262 the FAST station highlighted in magenta.

1263 **Figure 11.** (1) Rain rate (mm h^{-1}) during the night between the 4th and 5th of June (white dot is

1264 the position of the FAST station). These European radar composite products were provided by

1265   the Odyssey system, created in the framework of the Opera Program that is the radar component

1266   of the Eumetnet observation Program.

1267   **Figure 12.** MVP measurements across the FAST station. In the upper panel, the positions of

1268   each MVP cast (and of the FAST station) are shown as black (and red) crosses. Below are

1269   shown the sections of temperature (top), salinity (middle) and density (bottom).

1270   The map of the altimetry derived currents shows clearly the presence of the Algerian eddy west

1271   to the FAST station sampled during the MVP transect (figure 13).

1272   **Figure 13.** Geostrophic currents from satellite data with the Ekman component from WRF

1273   model added (black arrows, mean during the shown transect). In addition, in situ drifter

1274   trajectories during 30 days (launched at FAST and in its vicinity) are represented as white lines.

1275   Horizontal currents measured by the VM-ADCP for the first two bins (purple arrows -18 m,

1276   salmon arrows -26 m) are superimposed for comparison.

1277   **Figure 14.** ARIANE particles initial positions (white) and after a backward integration of 1

1278   (pink), 2 (light red), 3 (dark red), and 10 days (black) for the FAST station on the 3rd of June.

1279   (a) large view, (b) zoomed view, (c) ratio of particles remaining in the initial zone as a function

1280   of the number of backward integration days.

1281   **Figure 15.** Left panels: temperature-salinity diagram (upper panel), temperature profiles

1282   (middle panels), and profiles of beam transmission (lower panel). Right panels: evolution of

1283   the surface stratification (s_q, upper panel), salinity (anomalies to the profile of $t_o - 2^{nd}$ June

1284   16h30, middle panel) and chlorophyll fluorescence (lower panel) at the FAST station. Time

1285   Series are composed of 43 repeated CTD casts, with variable temporal resolution. The depth

1286   of the mixed layer is indicated by white dots. The time of the rainfall is indicated by the red

1287   line.

1288   **Figures 16.** Sea Surface Temperature during the cruise; left) outward route (10-28 May), right)

1289   return route (28 May-10 June). The daily satellite pixel data are used to produce a weighted

1290   mean. The weight for each pixel is calculated by normalizing by the square of the inverse

1291   distance from the pixel to the daily mean ship position. The ship track is shown in black, the

1292   short (long) station positions are indicated with black dots (squares). Data courtesy of

1293   L.Rousselet.

1294   **Figure 17.** As figure 17, but for the satellite-derived surface Chlorophyll-a concentration

1295   averaged over the entire duration of the cruise. Data courtesy of L.Rousselet.

1296   **Figure 18.** Nitrate (top right) and phosphate (bottom right; see Pulido-Villena et al., in prep.)

1297   concentrations (in nM) above 100 m, during the PEACETIME cruise along the west-east

1298   gradient shown on the map (left).

1299   **Figures**

1300   **FIG 1**
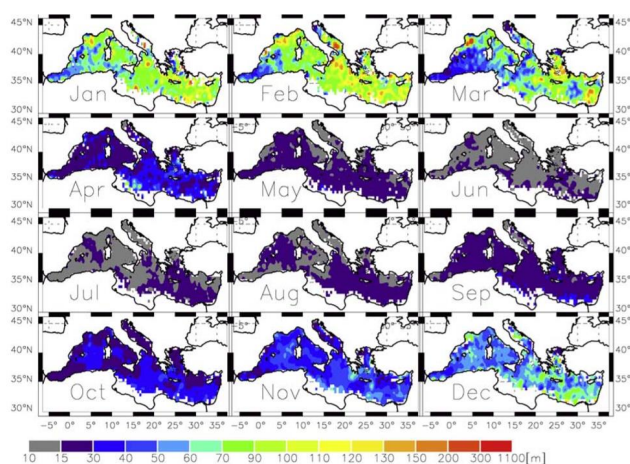
1301

1302

1303

FIG 2
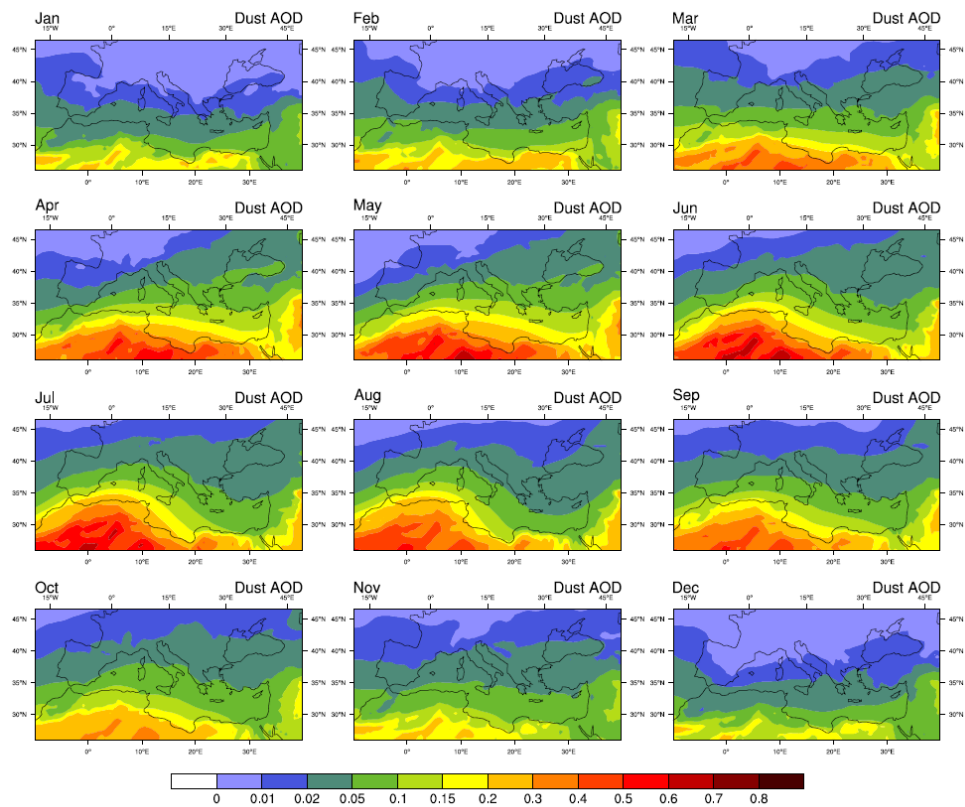
1304

1305

1306 **FIG 3**
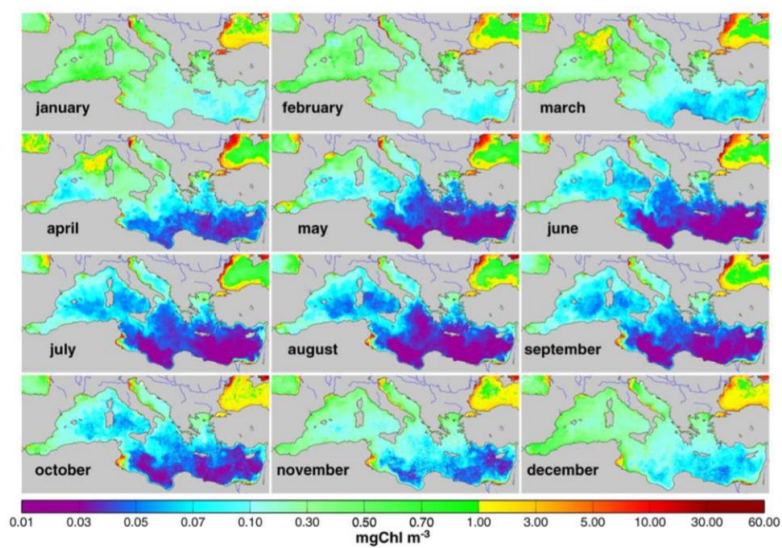
1307

1308 **FIG 4**
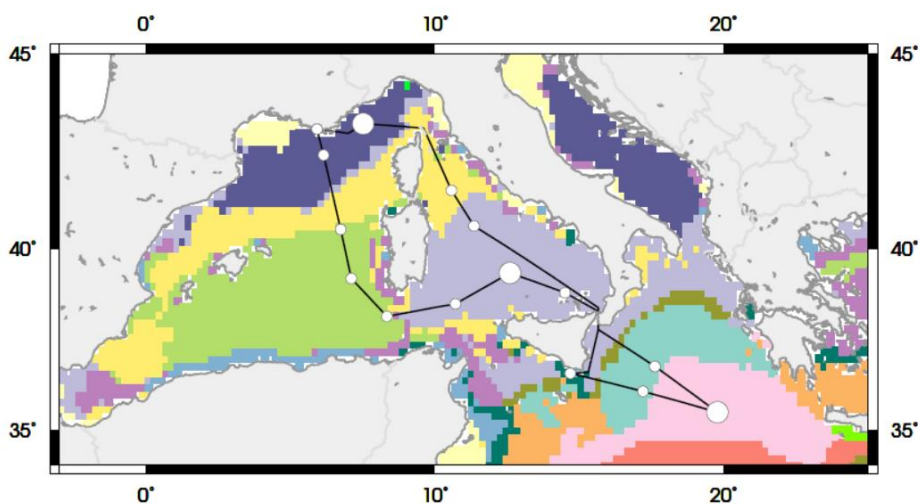
1309

1310

1311   **FIG 5**
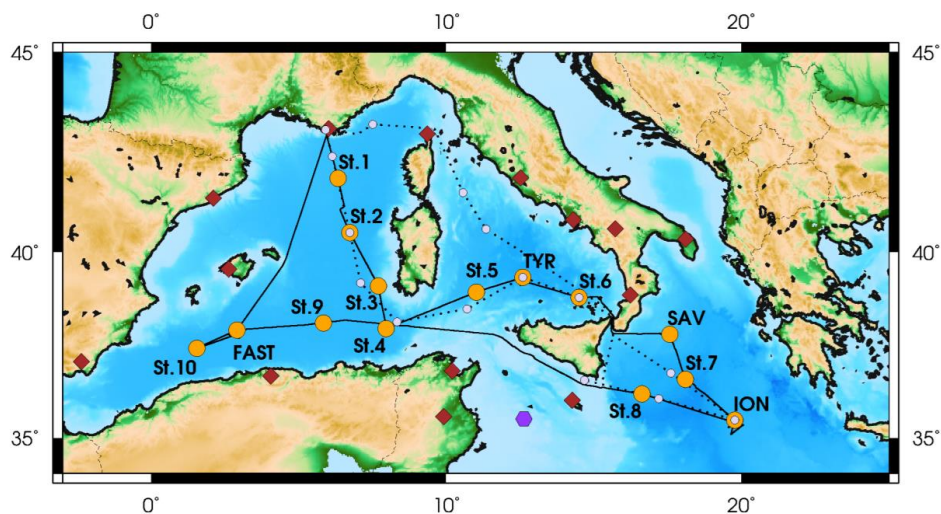
1312

1313   **FIG 6**
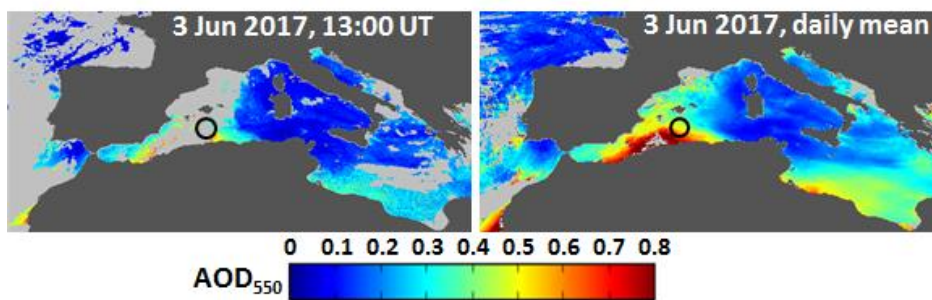
1314
1315

1316 **FIG 7**

1317

1318 **FIG 8**

1319

1320

1321   **FIG 9**

6-h accumulated dust deposition flux (mg m^{-2})

3 Jun, 12 UTC   3 Jun, 18 UTC   4 Jun, 18 UTC   5 Jun, 00 UTC

NMMB-BSC run of 02 Jun, 12 UTC

BSC-DREAM8b run of 02 Jun, 12 UTC

SKIRON run of 02 Jun, 12 UTC
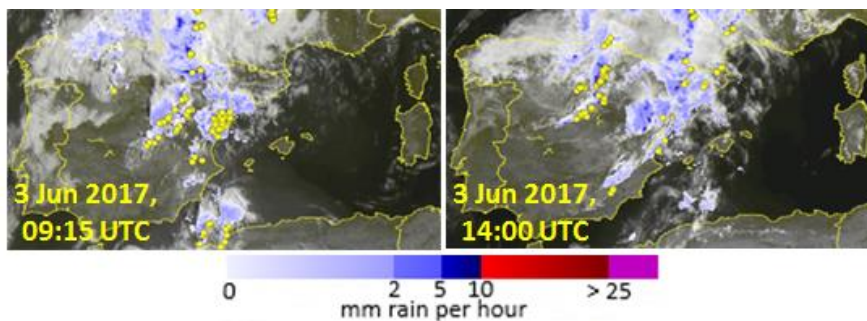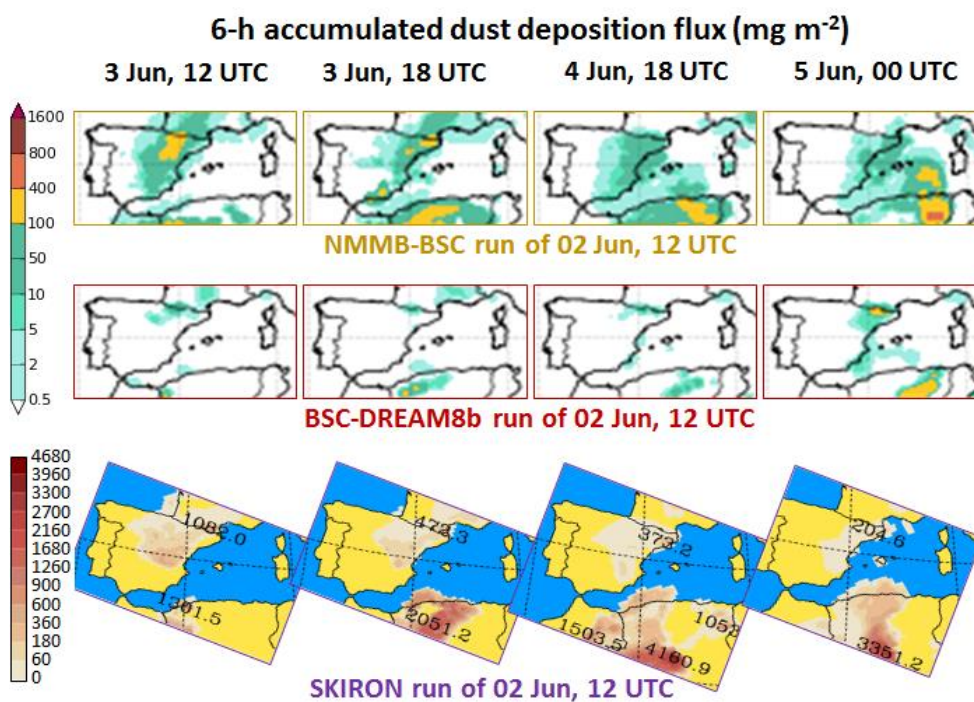
1322

1323   **FIG 10**
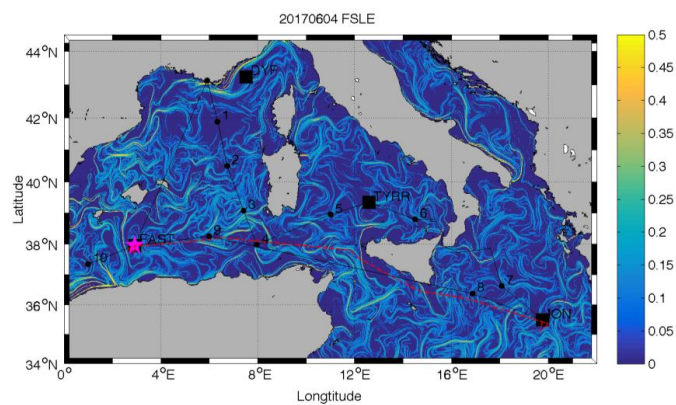
1324

1325

1326 **FIG 11**
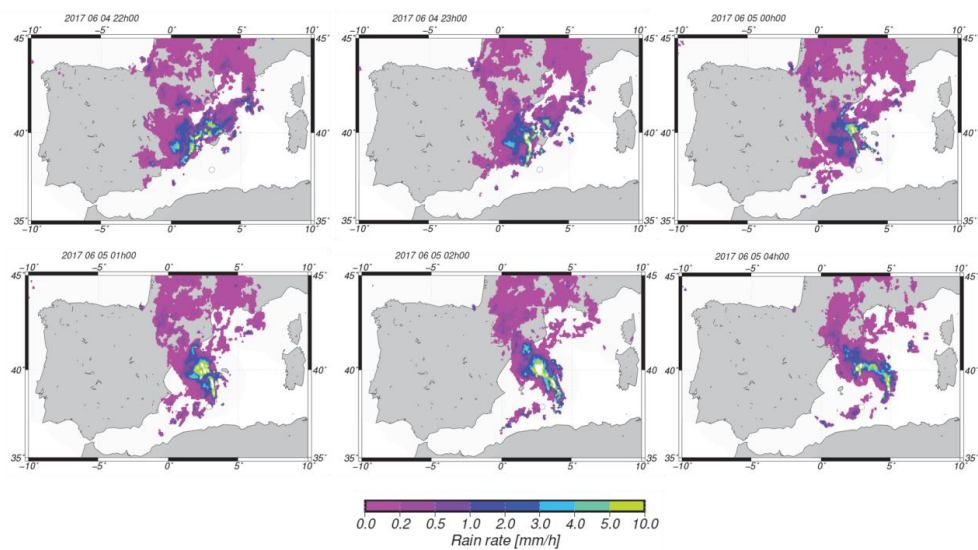
1327

1328

1329

FIG 12
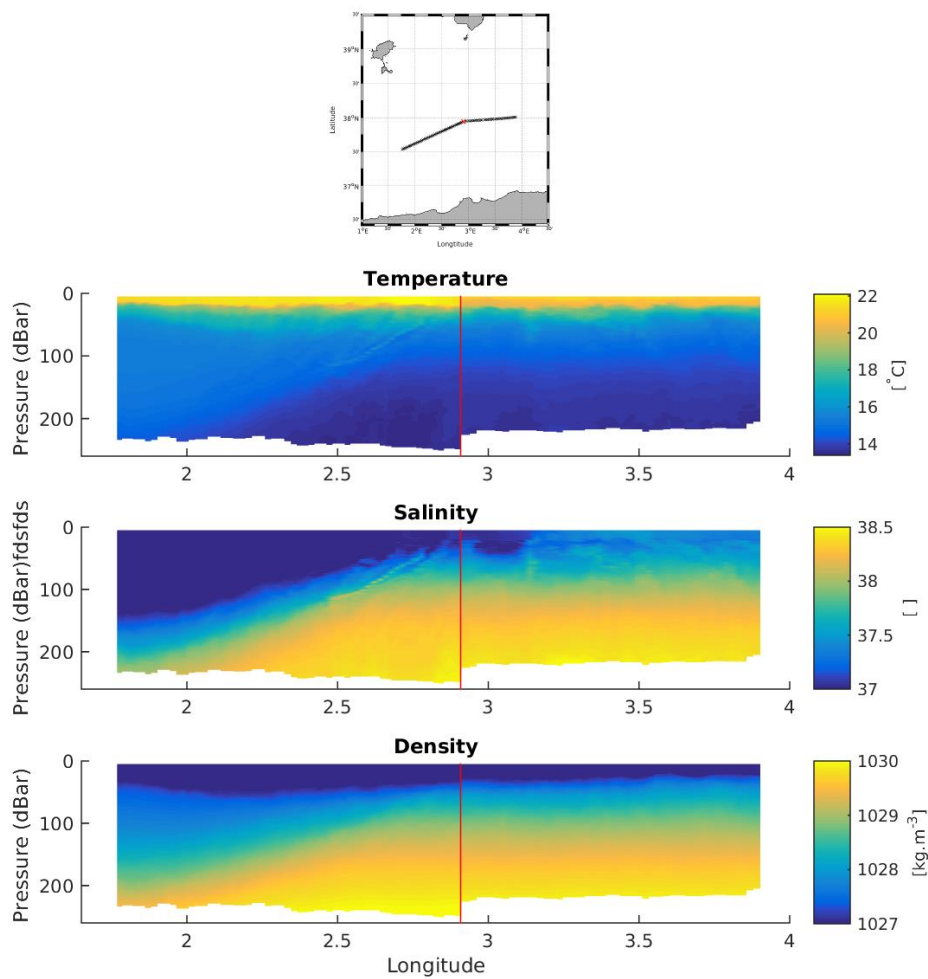
1330

1331

1332   **FIG 13**
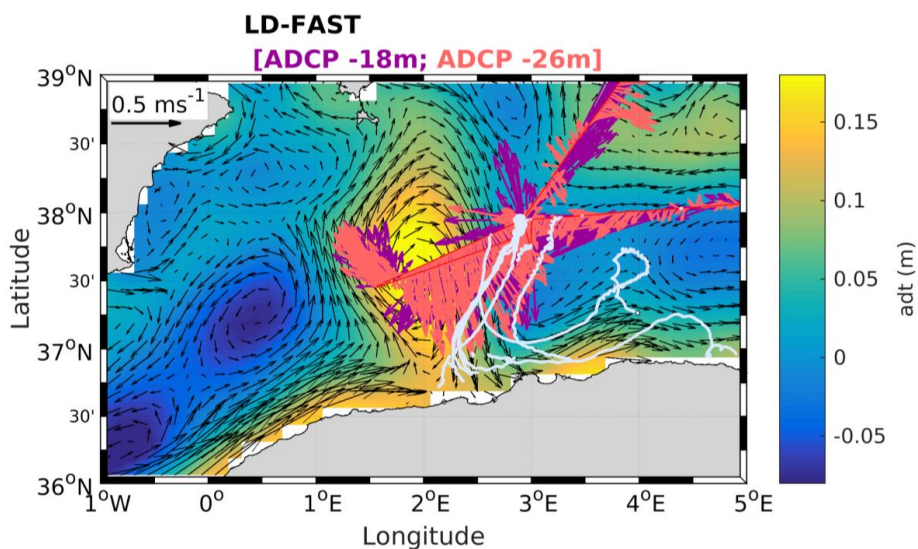
1333

1334   **FIG 14**
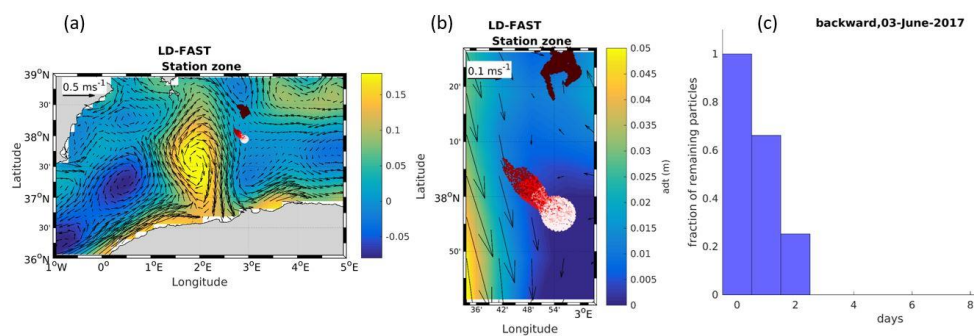
1335

1336

1337 **FIG 15**
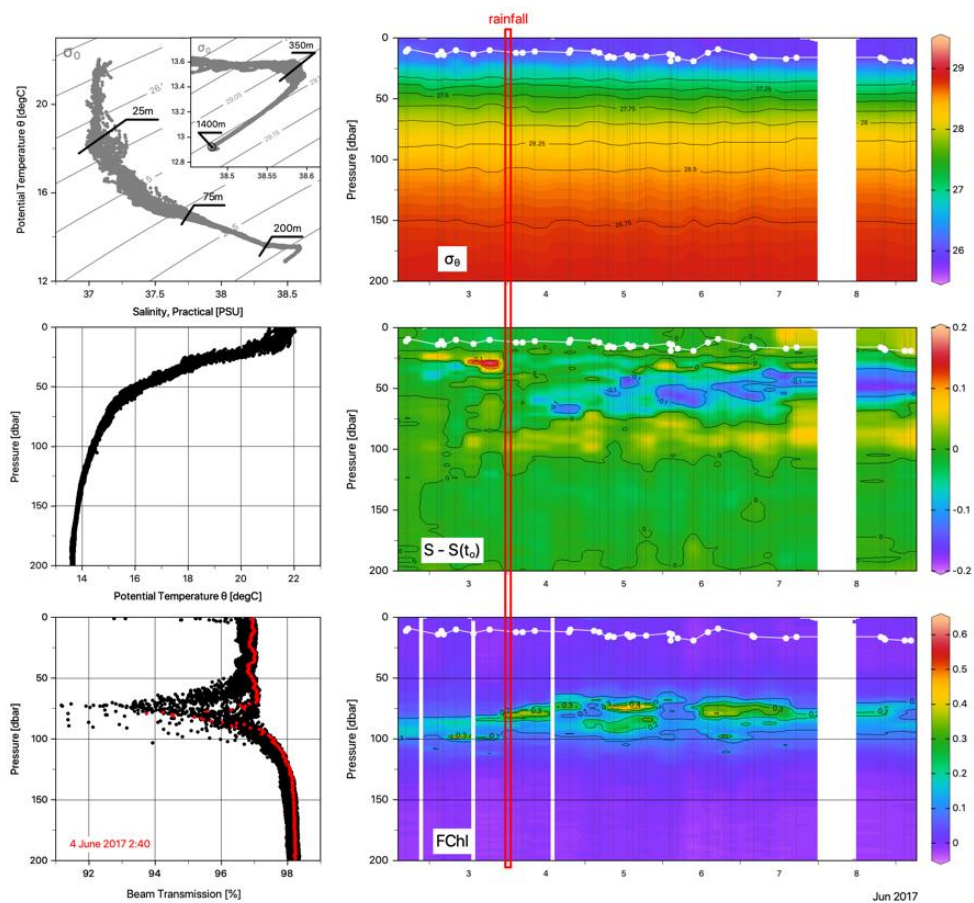
1338

1339 **FIG 16**
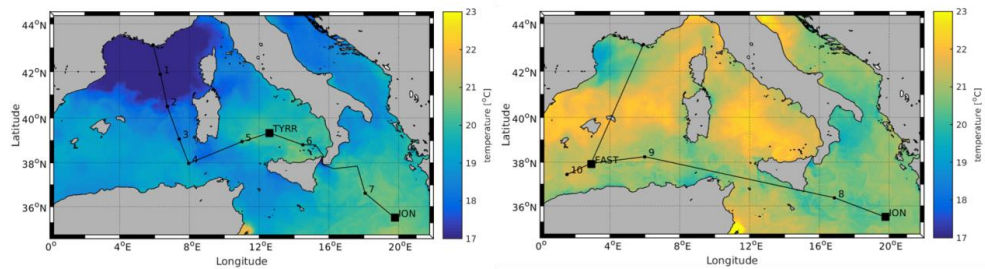
1340

1341

1342   **FIG 17**
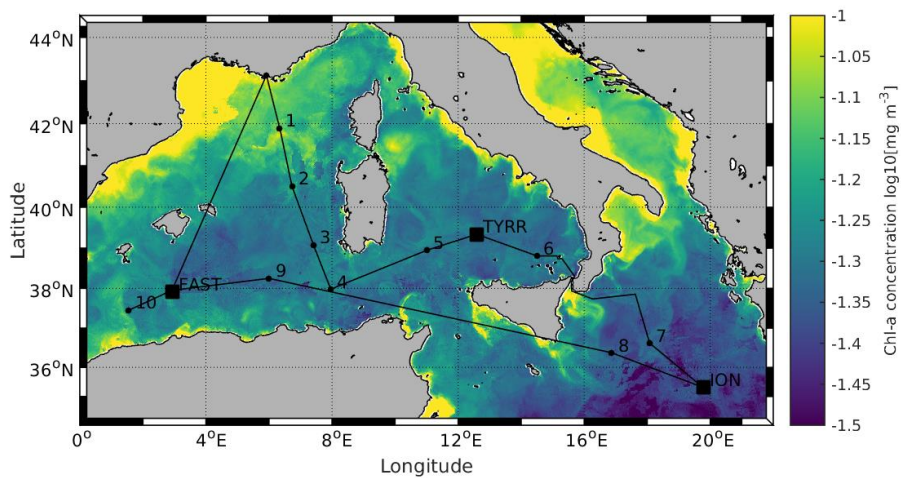
1343

1344

1345   **FIG 18**

1346